1. INTRODUCTION AND EXPLANATORY NOTES[1]

T. C. Moore, Jr.,[2] Philip D. Rabinowitz,[3] Peter Borella,[4] Anne Boersma,[3]
and
Nicholas J. Shackleton[5]

INTRODUCTION

The drilling plan for Leg 74 of the Deep Sea Drilling Project was designed to address three main scientific topics: (1) the history of the deep-water circulation in the southeastern Atlantic, (2) the nature and geologic evolution of the Walvis Ridge, and (3) the biostratigraphy and magnetic stratigraphy of this region. In order to study these subjects, a suite of five sites was drilled on the Walvis Ridge (Fig. 1; Table 1) that extended from its crest (near 1000 m water depth) down its northwest flank into the Angola Basin to a depth of 4400 m.

The sites are relatively close together and encompass a transect of approximately 230 km. They span a depth range of over 3 km and receive approximately the same rain of pelagic debris. Any site to site variation in average accumulation rates for a given interval of time should be a result of two main processes: (1) dissolution rate, which varies as a function of depth, and (2) winnowing and erosion, which may also vary as a function of depth and are likely to be important near large topographical features. Detailed stratigraphic studies and the analysis of the accumulation rates for different size components aid in distinguishing these two processes.

Most classical marine biostratigraphies were established for tropical sequences; the present suite of sites serves to establish stratigraphies for more temperate latitudes. The usefulness of this material is enhanced by the recovery of several sections within a relatively small geographic area and by the use of the newly developed Hydraulic Piston Corer (HPC) in three of the five sites. Complete coring of several sites within a small area assures nearly complete recovery of the biostratigraphic sequence as well as optimal preservation of both the older parts of the section (in deeper sites with less overburden and diagenesis) and the younger parts of the section (in shoaler sites with less dissolution). The HPC is designed to recover relatively undisturbed cores in the upper, unlithified part of the section, thus providing the opportunity for detailed studies of biostratigraphy; paleomagnetism; physical properties; and biotic, geochemical, and lithologic time series.

Our knowledge of aseismic ridges in general, and of the Walvis Ridge in particular, is also enhanced by this transect. First it allows us to test our hypotheses concerning the age and subsidence history of the Ridge, and second, it provides a lateral sequence of samples of the upper basement complex. These samples allow us to study the magnetic character, petrology, and chemical composition of the crustal rocks as well as the mode of emplacement of the basement complex.

OCEANOGRAPHIC SETTING

All sites lie beneath the generally northward-flowing surface currents in the eastern part of the central subtropical gyre and are approximately 800 km off the coast of Africa, well outside the main flow of the eastern boundary current (Benguela Current) and the associated regions of high productivity. With the exception of storm-induced currents, near-surface conditions are rather uniform over the study area and are assumed to have remained so in the past. Even if surface current patterns changed significantly in the past, at any given time all the sites within this relatively small study area are expected to have received a nearly uniform supply of biogenic and detrital material.

All sites in this region are above the 5-km-deep carbonate lysocline as defined by Berger (1974). Only Sites 527 and 528 lie near both the level of "perceptible dissolution" (R_o level of Berger, 1977) and the calcite saturation level of Takahashi (1975), which in the southeastern Atlantic are thought to be close to 4 km. The shallowest site (526, at 1054 m) lies within the depth interval presently occupied by Antarctic Intermediate Waters (AAIW). The remaining, deeper sites are located at depths ranging from approximately 2500 to 4400 m (Table 1). They are all within the depth interval occupied by North Atlantic Deep Water (NADW), which presently dominates the deep and bottom waters of the Angola Basin. The Walvis Ridge, together with the Mid-Atlantic Ridge, form an effective topographic barrier which largely isolates the Angola Basin from the Antarctic Bottom Water (AABW) to the south and west. Only a small amount of AABW enters the Angola Basin through the two deepest passages: the Romanche Fracture Zone, near the equator (Wüst, 1936), and the Walvis Passage, near the southwestern end (36°S, 7°W) of the Walvis Ridge (Connary and Ewing, 1974). Geologic evidence from previous Deep Sea Drilling legs (Legs 3, 40, and

[1] Moore, T. C., Jr., Rabinowitz, P. D., et al., *Init. Repts. DSDP*, 74: Washington (U.S. Govt. Printing Office).
[2] Graduate School of Oceanography, University of Rhode Island, Kingston, Rhode Island.
[3] Lamont-Doherty Geological Observatory, Columbia University, Palisades, New York. Present addresses: Rabinowitz, Department of Oceanography, Texas A&M University, College Station, TX; Boersma, P.O. Box 404, R.R. 1, Stony Pt., NY 10980.
[4] Deep Sea Drilling Project, Scripps Institution of Oceanography, La Jolla, California.
[5] Godwin Laboratory, University of Cambridge, Cambridge, CB2 3RS, United Kingdom.

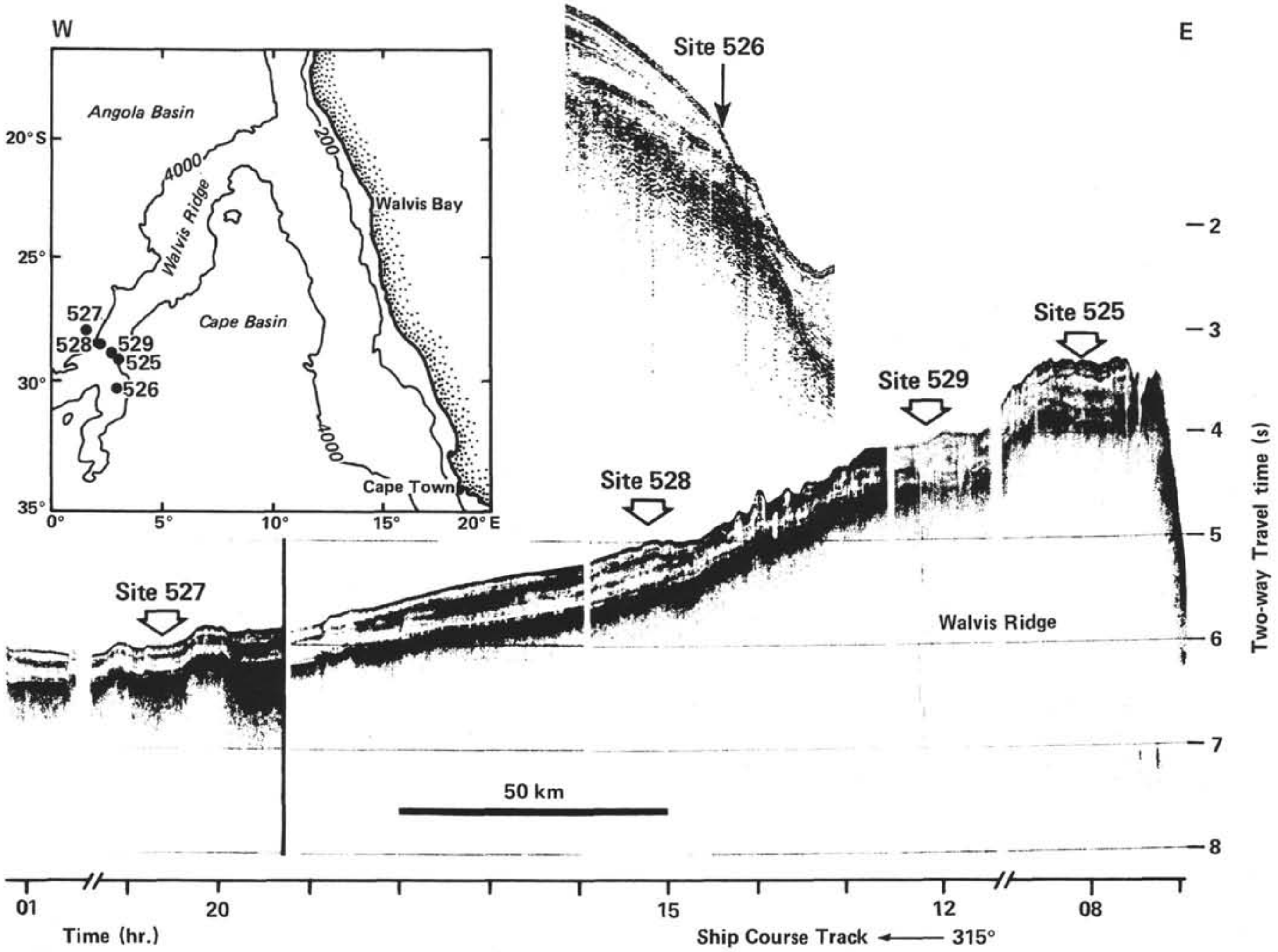

Figure 1. Site localities and index map.

Table 1. Leg 74 coring summary.

Hole	Date (1980)	Latitude	Longitude	Water Depth (m)[a]	Penetration (m)	Number of Cores	Length Cored (m)	Length Recovered (m)	Recovery (%)
525	10 June	29°04.24′S	02°59.12′E	2467	3.6	1	3.6	3.6	100
525A	10–15 June	29°04.24′S	02°59.12′E	2467	678.1	63	555.1	406.7	73
525B	15–19 June	29°04.24′S	02°59.12′E	2467	285.6	53	227.0	181.7	80
526	14 July	30°07.36′S	03°08.28′E	1054	6.3	2	6.3	3.6	57
526A	14–16 July	30°07.36′S	03°08.28′E	1054	228.8	46	200.8	206.6	100+
526B	16 July	30°07.36′S	03°08.28′E	1054	28.3	5	22.0	13.5	61
526C	16–17 July	30°07.36′S	03°08.28′E	1054	356.0	21	185.0	70.9	38
527	28 June–4 July	28°02.49′S	01°45.80′E	4428	384.5	44	384.5	243.9	63
528	4–10 July	28°31.49′S	02°19.44′E	3800	555.0	47	441.0	272.8	62
528A	10–13 July	28°31.16′S	02°18.97′E	3815	130.5	30	130.5	116.5	89
529	18–20 July	28°55.83′S	02°46.08′E	3035	417.0	44	417.0	309.7	74
					Totals	356	2572.8	1829.5	71

[a] Water depths from sea level.

73) suggests that the chemical character of the deep and bottom waters of the Angola Basin changed markedly through the Cenozoic.

GEOLOGIC SETTING

The Walvis Ridge consists of offset NNW-trending crustal blocks connected by ENE-trending blocks. Together these segments form a roughly linear ridge which extends to the northeast from the Mid-Atlantic Ridge and joins the continental margin of Africa near 20°S latitude. Within the area of study (Figs. 1 and 2), structural blocks tend to slope steeply into the Cape Basin and to slope more gradually northwestward into the Angola Basin.

Until recently it was uncertain whether the Walvis Ridge was an ocean crustal feature or a fragment of

Figure 2. Bathymetry.

continental crust which had been separated from the main continental blocks during the early phases of rifting in the South Atlantic. Seismological and gravity studies indicate that the average crustal thickness beneath the ridge is 12 to 15 km and that the seismic character of the crust is consistent with an oceanic origin (Chave, 1979; Detrick and Watts, 1979; Goslin and Sibuet, 1975). Recent geophysical surveys of the study area (Rabinowitz and LaBrecque, 1979; Rabinowitz and Simpson, 1979) identified Magnetic Anomaly 32 (lower Maestrichtian) near the crest of the Walvis Ridge, with younger anomalies extending to the west into the Angola Basin. These results lend support to the idea that the Walvis Ridge was formed at a mid-ocean ridge by seafloor spreading processes.

Site 526, the shoalest site, is located near the crest of what appears to be a separate structural block. It lies to the south of the block on which the remaining four sites in the transect were drilled (Figs. 1 and 2). Site 525 is located near the crest of the more northern block, in an area with nearly 600 m of sediment. Site 529 is the next deeper site and lies on the eastern flank of a valley which forms a saddle in the ridge. Sites 528 and 527 are in progressively deeper waters and have somewhat thinner sedimentary sections.

Acoustic basement in the study area is comparatively smooth, with pronounced basement highs occurring mainly in the crestal regions. There appear to be at least three sub-bottom reflectors defining four sedimentary intervals which can be traced through the area. The section beneath the deepest sediment reflector thins downslope and nearly merges with the basement reflector in the area of Site 527 (Fig. 1). The next shoaler interval appears to be of approximately constant thickness throughout the transect, whereas the one above that (third from the bottom) appears to pinch out between Sites 528 and 527. The shoalest interval is dissected between Sites 529 and 528 and thins between Sites 528 and 527. The reflection records taken near the edges of the crestal region and near the valley to the west of Sites 525 and 529 show evidence of erosion and slumping in the study area.

Sediments are composed mainly of calcareous oozes ($\geq 90\%$ $CaCO_3$). Because of the predominance of NADW in most of the Angola Basin, the calcite compensation depth presently lies below 5500 m (Berger and Winterer, 1974). The noncarbonate fraction is dominated by clay, with very little or no biogenic opal.

SEDIMENTOLOGY AND LITHOSTRATIGRAPHY

The overwhelming majority of sediments recovered from Sites 525–529 are calcareous oozes and chalks. Nannofossils and foraminifers are the dominant microfossils identified. Four major lithostratigraphic units are recognized and are discussed in the following paragraphs in order of descending depth.

Nannofossil and foraminifer-nannofossil oozes (Unit I) dominate the upper 150–250 m in each hole (Figs. 3–7). $CaCO_3$ content is well over 90%. Primary and secondary sedimentary structures are very poorly preserved. These calcareous oozes are the only sediment type which can be directly correlated from hole to hole, indicating a similar and uniform sediment source over the study area since approximately the late Oligocene. The only exception to this is at the base of Site 527, where pelagic clay ($CaCO_3$ content approximately 20%) occurs in two distinct beds (Fig. 7). These beds, with their poorly preserved calcareous microfossils, indicate intervals of time when the CCD was elevated. Some slumps were recognized within the oozes with the aid of very precise biostratigraphic age determination. In addition, slump deposits were also clearly seen in seismic sections (Fig. 8).

The uppermost unit grades into alternating ooze and chalk (Unit II) for approximately 100 m, with ooze dominant at the top and chalk dominant toward the base of the unit. $CaCO_3$ content is still over 90%, but preserva-

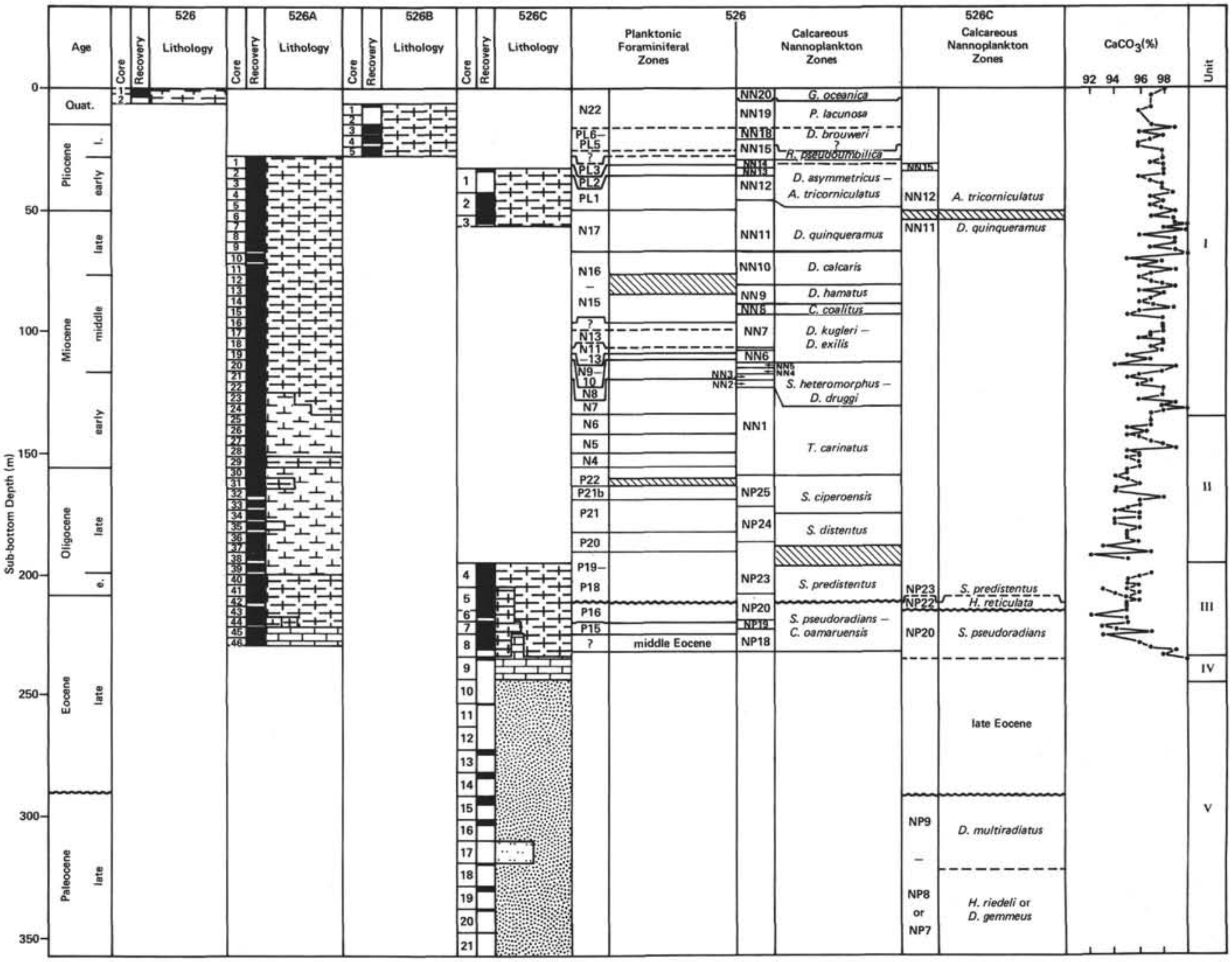

Figure 3. Site 526 stratigraphic summary (see Fig. 4 for symbols used).

tion of biogenic sedimentary structures is moderate to good. This preservation is directly related to the chalk content. The poor preservation of sedimentary structures in the overlying ooze unit is thus probably the direct result of drilling. Stratigraphically the ooze-chalk sequence can be correlated from site to site with the exception of Site 526, the shoalest site, where there is only about 30 m of chalk alternating with ooze. The age of the ooze-chalk interval ranges from early Oligocene to late Paleocene at the three intermediate depth sites (525, 529, and 528).

Site 526 is located on another crustal block (Rabinowitz and Simpson, 1979), which during the early Oligocene to late Eocene was very close to sea level. The presence of shallow-water fossils (e.g., oysters, clams) and algal oncolites, together with graded sequences of rubbly limestones tentatively interpreted as a channel fill, support the assumption of a shallow-water, high-energy environment in which oozes and chalks could not accumulate because of the winnowing action of waves and currents.

At Site 527 the base of the ooze-chalk sequence is late Paleocene in age, which agrees well with the other sites. However, the Oligocene age sediments are drastically reduced in thickness because of dissolution (see Sedimentation History, this chapter). Thus the upper boundary of the ooze-chalk sequence at Site 527 is not synchronous with the top of the ooze-chalk sequences at the other sites.

The ooze-chalk sequence passes gradually into Unit III chalks and highly indurated chalks, which continue to basement basalt. Within this unit, $CaCO_3$ content is extremely variable (20-80%). Although the decrease in $CaCO_3$ is atrributed primarily to increasing amounts of volcanogenic materials and dissolution, there were also cyclic sedimentation patterns. A spectacular turbidite sequence is preserved at the base of this unit, just above the basement/sediment contact at Hole 525A. In addition, many other small-scale slumps and cycles of turbidites are present at Sites 525, 527, 528, and 529. The increased frequency of evidences of slumping and volcanic activity toward the bottom of the unit indicates a change in sedimentation from a dominantly pelagic to a relatively shallow-water, volcaniclastic mode. Volcaniclastic layers and ash layers are well preserved. However, the ash layers cannot be directly correlated from hole to hole. Beautifully preserved primary and secondary sedimentary structures are present throughout the entire unit. Some of the better-preserved structures are graded bedding, cross laminations, convolute bedding, and microfaults. Biogenic sedimentary structures are ubiquitous and indicate that the sediments have been reworked at least once since deposition. *Zoophycos*, *Planolites*, and *Chondrites* are the most abundant ichnogenera present.

Stratigraphically, Unit III varies in thickness from 175 m in Hole 525A to approximately 110 m in holes at Sites 527, 528, and 529, with ages ranging from late Paleocene to Late Cretaceous. Excluding Site 526, where Unit III chalks are absent, the chalks are easily traceable from site to site both stratigraphically and seismically. Chert nodules and/or beds are found in the lower portions of Units II through III but are confined to Sites 525, 528, and 529; the shoalest and deepest sites contain no chert. Although the cherts are confined to a certain lithostratigraphic interval, we can make no direct correlation of chert beds from site to site. They probably formed as a result of a silica-rich solutions migrating through permeable layers into pockets or voids and eventually crystallizing as chert.

The much-studied Tertiary/Cretaceous boundary occurs within Lithostratigraphic Unit III. At four of the sites (525A, 527, 528, 529) the Tertiary/Cretaceous boundary is found in zones of high slump activity, turbidity deposits, and low carbonate concentrations (Figs. 4-7). Quite possibly the high tectonic or current activity evidenced here may have been associated with the worldwide terminal Cretaceous event.

In place of the chalks, volcaniclastic sediments, and structural slumps, Site 526 contains calcareous sands consisting of approximately 60% carbonate and 40% noncarbonate grains. The noncarbonate fraction contains angular quartz, feldspar grains (K-feldspar), and volcanic rock fragments. Recovery of this sand was very poor, with total drilling penetration only approximately 110 m. Drilling was terminated owing to unstable hole conditions. The immature sands indicate that a very shallow water, high-energy condition existed at or very near Site 526 from late Eocene to late Paleocene. Shallow-water mollusk, echinoderm, and bryozoan fragments are found within the unit but may be contamination from overlying units.

At three sites, 525, 528, and 527 (Figs. 4, 6, 7), basement was penetrated. Interbedded with the basalts are sedimentary rocks of varied lithologies. Marly nannofossil chalks, limestones, mudstones, and siltstones are the major rock types. Sediment layer thicknesses range from a few centimeters to several meters. Primary and secondary sedimentary structures are abundant and very well preserved. They are the same as those in Unit III. Fairly shallow water fossils—for example, *Inoceramus*—are also present. Many of the interbeds are identified as small-scale slump or turbidite deposits. Interstitial pore water analyses of Ca and Mg concentrations show a dramatic inverse relationship. For example, at Site 528, Ca concentration in pore water increases from 26.3 mM/l above basement to 76.52 mM/l in the sedimentary interlayers within the basement. Conversely, magnesium decreases from 39.33 mM/l above basement to 1.20 mM/l in the basement sedimentary interlayers. It appears that this rapid change is due to seawater-basement interaction, possibly at elevated temperatures (Bischoff and Dickson, 1975). Magnesium is released during submarine weathering of basalt and combines with CO_3 to form a precipitant, aiding in the cementation process. Thus magnesium is depleted in pore waters. Calcium, however, is enriched because of dissolution and weathering of basalt. The "baked" appearance of many of the in-

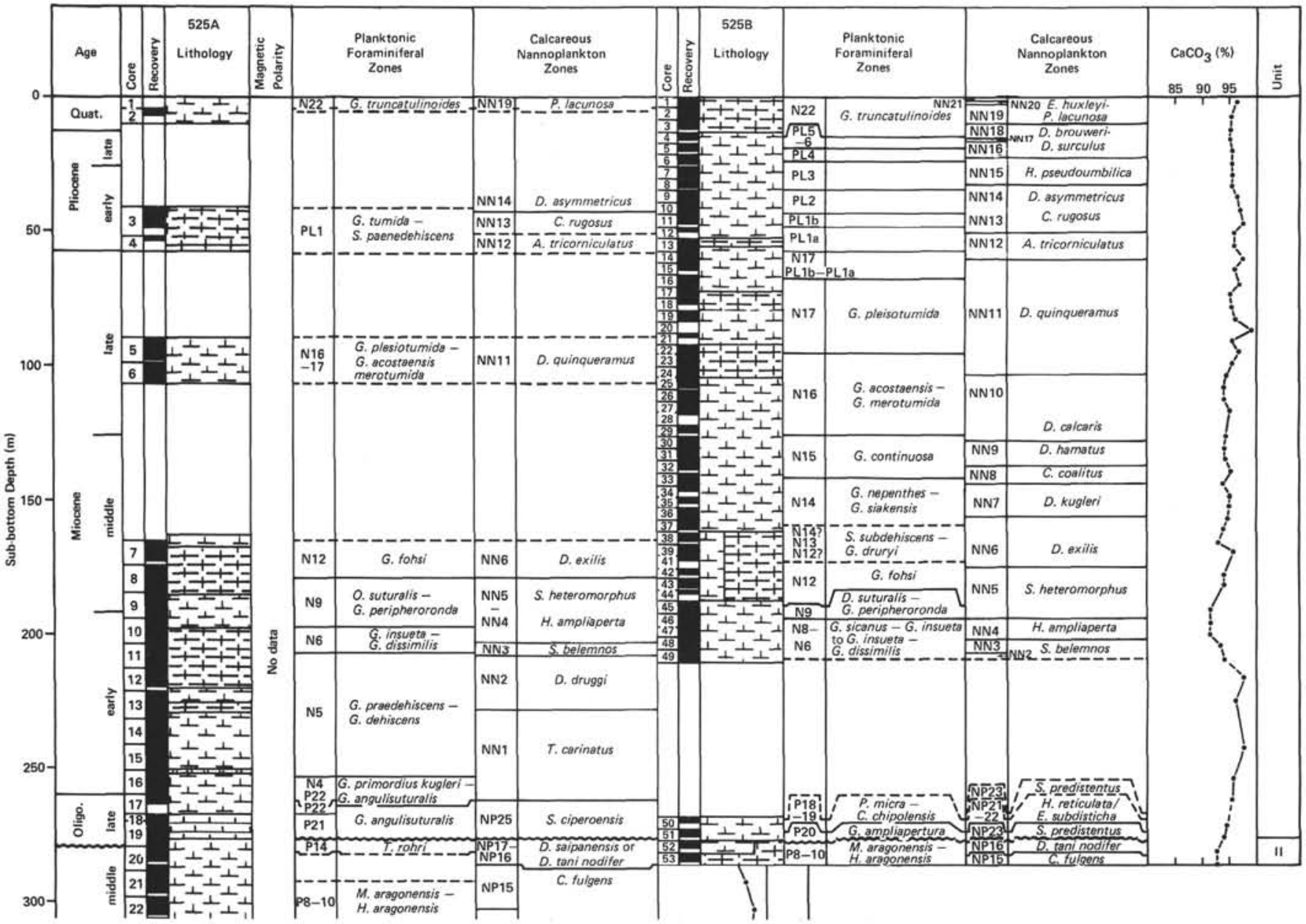
Age
Core
Recovery
525A
Lithology
Magnetic Polarity
Planktonic Foraminiferal Zones
Calcareous Nannoplankton Zones
525B
CaCO3 (%)
85 90 95
Unit
Sub-bottom Depth (m)
0
50
100
150
200
250
300
Quat.
Pliocene
Miocene
Oligo.
late
early
middle
No data
N22 G. truncatulinoides
NN19 P. lacunosa
NN14 D. asymmetricus
PL1 G. tumida – S. paenedehiscens
NN13 C. rugosus
NN12 A. tricorniculatus
N16–17 G. plesiotumida – G. acostaensis merotumida
NN11 D. quinqueramus
N12 G. fohsi
NN6 D. exilis
N9 O. suturalis – G. peripheroronda
NN5 S. heteromorphus
NN4 H. ampliaperta
N6 G. insueta – G. dissimilis
NN3 S. belemnos
NN2 D. druggi
N5 G. praedehiscens – G. dehiscens
NN1 T. carinatus
N4 G. primordius kugleri
P22 G. angulisuturalis
P21 G. angulisuturalis
NP25 S. ciperoensis
P14 T. rohri
NP17–NP16 D. saipanensis or D. tani nodifer
NP15 C. fulgens
P8–10 M. aragonensis – H. aragonensis
NN21
N22 G. truncatulinoides
NN20 E. huxleyi- P. lacunosa
NN19
NN18
NN17 D. brouweri- D. surculus
NN16
PL5–6
PL4
PL3
NN15 R. pseudoumbilica
PL2
PL1b
PL1a
N17 PL1b–PL1a
N17 G. pleisotumida
N16 G. acostaensis – G. merotumida
NN10
D. calcaris
N15 G. continuosa
NN9 D. hamatus
NN8 C. coalitus
N14 G. nepenthes – G. siakensis
NN7 D. kugleri
N14? N13 N12? S. subdehiscens – G. druryi
N12 G. fohsi
D. suturalis – G. peripheroronda
N8–N6 G. sicanus – G. insueta to G. insueta – G. dissimilis
NN2
P18–19 P. micra – C. chipolensis
P20 G. ampliapertura
NP23 S. predistentus
NP21–22 H. reticulata/ E. subdisticha
NP23 S. predistentus
NP16 D. tani nodifer
NP15 C. fulgens
II

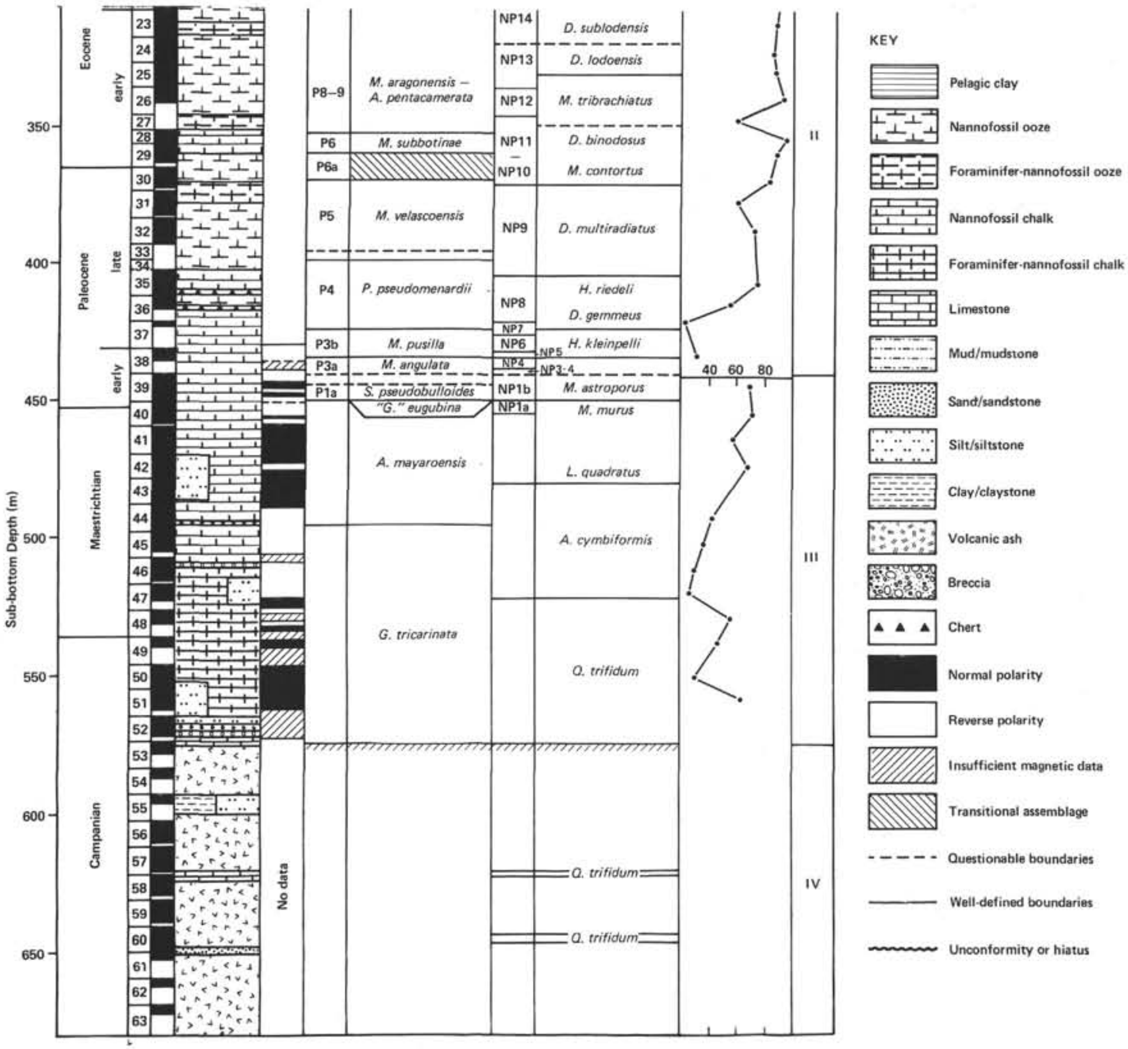

Figure 4. Stratigraphic summary, Holes 525A and 525B.

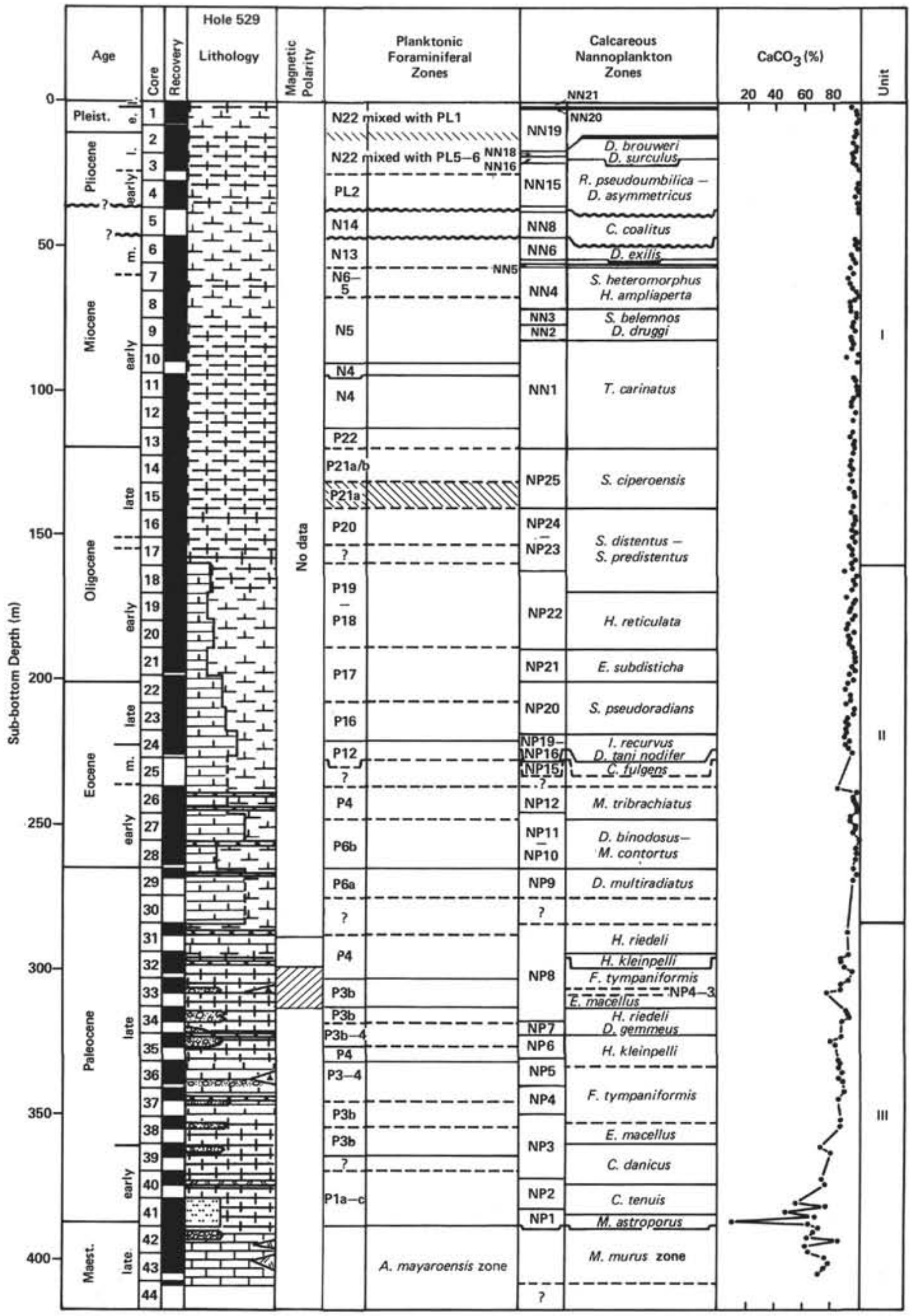

Figure 5. Stratigraphic summary, Site 529 (see Fig. 4 for symbols used).

terlayers, especially near the contact with basalts, also supports the possibility of seawater–basalt exchange at higher than ambient temperatures.

PHYSICAL PROPERTIES

Gravimetrically determined wet-bulk density and wet-water content, shrinkage (i.e., loss of volume by drying at 110°C), shear strength, sonic velocity, and thermal conductivity were routinely determined on samples taken from the least disturbed sections of the recovered material. In spite of the site to site differences in water depth and physical setting, the results show a distinct trend of slowly increasing diagenesis with depth below seafloor which is quite similar at all five site locations. This similarity in physical properties is not surprising, since the sequences of sediment types from site to site were also similar.

The general results and trends of the main physical properties in the different lithologic units are shown in Table 2.

In the upper 50 m below seafloor, the oozes are unconsolidated. The uppermost samples have very high water content and porosity and very low wet-bulk density. From 30 to 50 m sub-bottom, the water content and porosity decrease and wet-bulk density increases. Below that depth, no large changes occur in the ooze unit. Sonic velocity is very uniform throughout this unit.

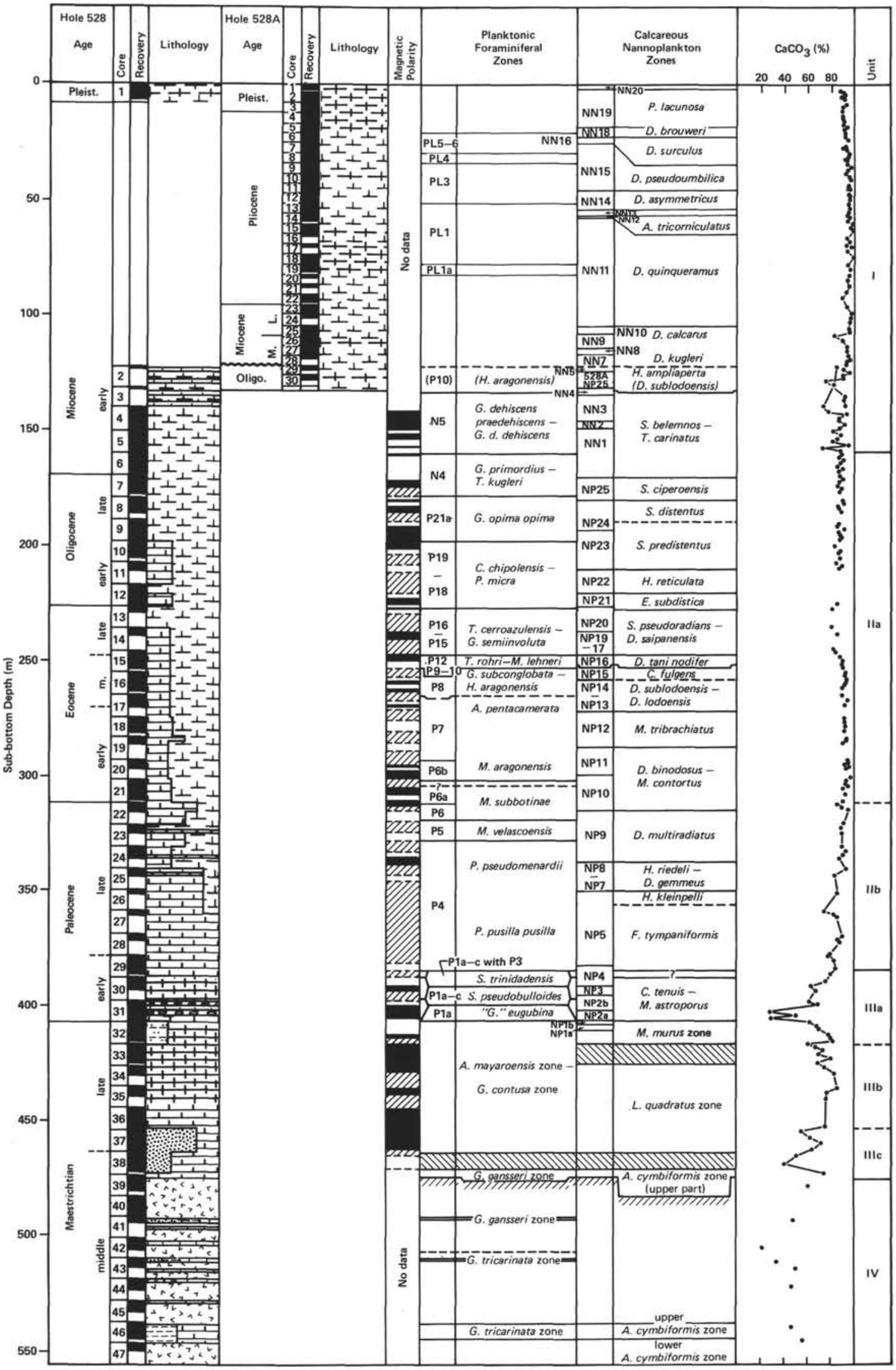

Figure 6. Stratigraphic summary, Site 528 (see Fig. 4 for symbols used).

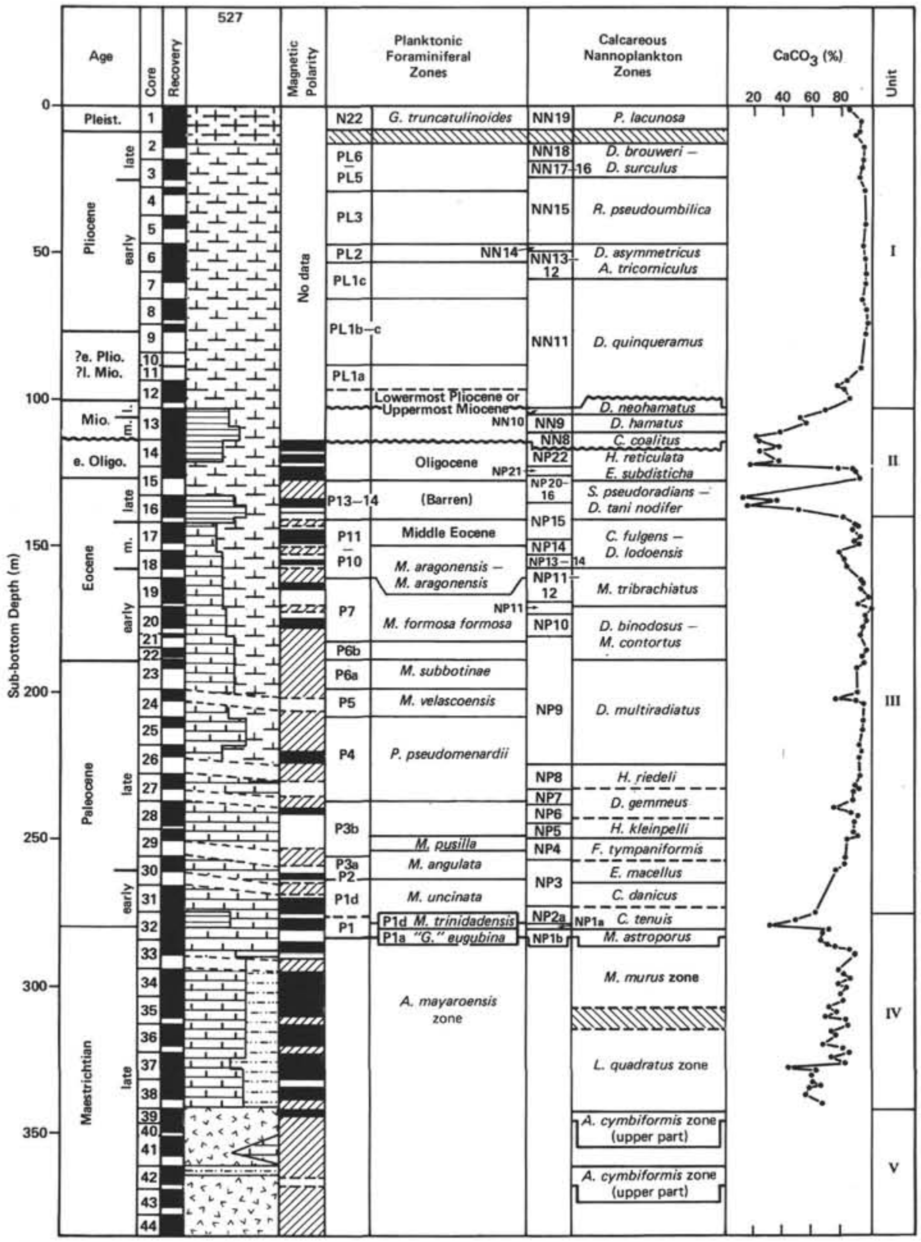

Figure 7. Stratigraphic summary, Site 527 (see Fig. 4 for symbols used).

The next obvious change in the physical properties occurs in the transitional ooze–chalk zone. The water content and porosity decrease distinctly, and the wet-bulk density and sonic velocity increase. This trend continues into the next-deeper unit, which is primarily chalk.

Generally there is a larger data scatter in the chalk unit, owing to variable lithology, especially in the lower part, where chalks are interbedded with volcanogenic material.

The determination of shrinkage and shear strength of the sediments was possible only in the upper two units (ooze and transition ooze–chalk). In the ooze unit there is little change in shrinkage with sub-bottom depth, and shear strength is very low. In the transition zone, however, there are obvious changes; shrinkage decreases to zero and shear strength increases dramatically. Both effects show the result of increasing compaction, which transforms the oozes into firm chalk layers.

Thermal conductivity measurements show a wide scatter of values in all the lithologic units. In a few places, there is a slight trend of increasing conductivity with depth.

Physical property measurements were also made on a few unusual lithologic units (Table 2). For example, at Site 527 a unit of pelagic clay and clayey ooze occurred between the ooze and transition ooze–chalk units. For this unit, shrinkage and shear strength were much higher than in the carbonates.

IGNEOUS PETROLOGY

Although aphyric basalts occur at all three sites, moderately to highly phyric varieties are restricted to the two flank sites. Significant compositional differences

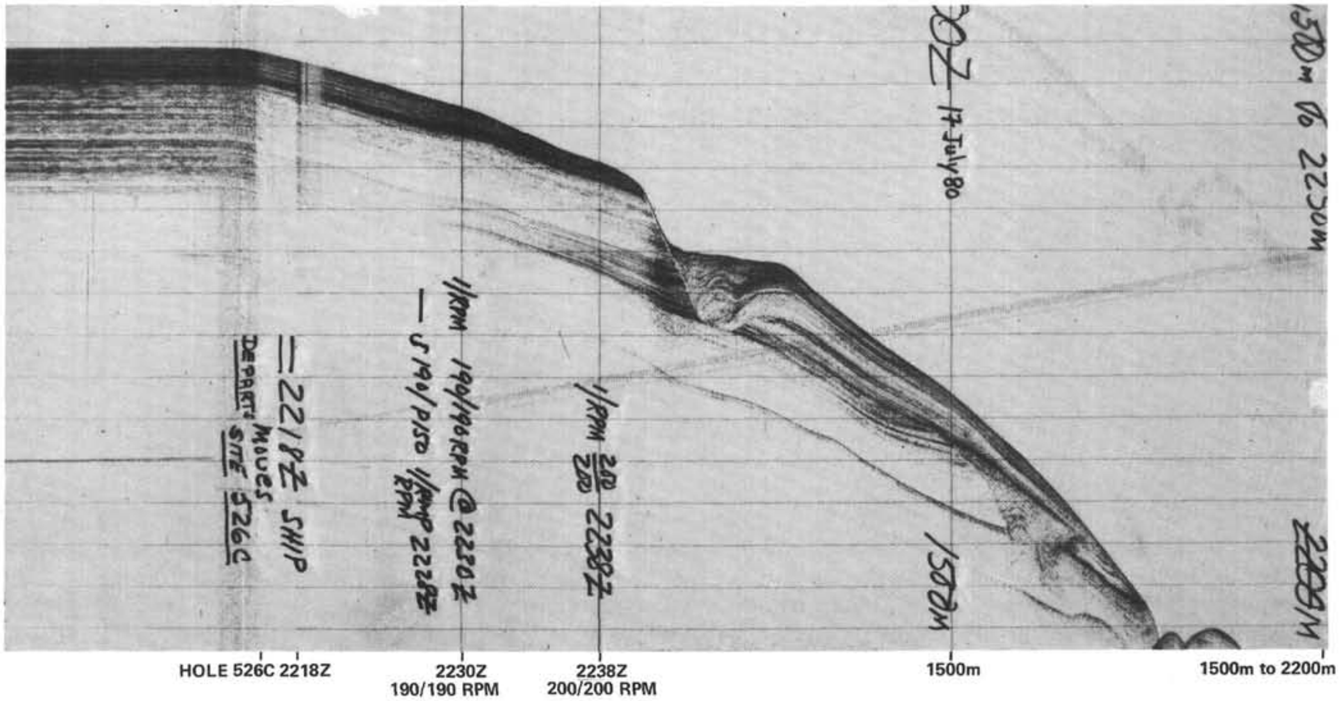

Figure 8. 3.5-kHz seismic record of a small-scale slump departing Site 526.

Table 2. Summary of physical properties.

	Site	Oozes: 0–50 m Sub-bottom	Oozes: Below 50 m	Clay and Clayey Oozes	Transition Ooze-Chalk	Chalks	Basement: Sediments	Basement: Basalt	Site
Wet-bulk density (gm/cc)	525	1.67→1.71	1.75		1.75→2.05	2.05	(1.93)	2.47	525
	526	1.7	1.7→1.75						526
	527	1.62→1.75	1.75	1.75	1.75→1.9	1.9→1.95	(2.05)	2.64	527
	528	1.62→1.73	1.73→1.81		1.81→2.0	2.0→2.05	2.05	2.85	528
	529	1.75	1.75		1.75→1.9	1.95→2.2			529
Wet-water content (%)	525	36→34	33→30		30→22	22→16	(28)	8	525
	526	40→34	34→30						526
	527	40→33	34	35	34→28	28→25	(21)	5	527
	528	42→34	34→31		31→24	24→20	22	4	528
	529	33	33		33→26	26→15			529
Porosity (%)	525	60→57	56		50→40	40→35	(53)	20	525
	526	60	60→53						526
	527	64→57	57	57	55→50	47	(42)	13	527
	528	65→56	56→53		53→45	45→41	43	10	528
	529	55	55		55→45	45→31			529
Sonic velocity (km/s) (horizontal)	525	1.6	1.6		1.6→1.9	1.9→2.6	1.8	3.9	525
	526	1.6	1.6						526
	527	1.53	1.53	1.55	1.55→1.7	1.7	1.9	4.4	527
	528	1.55	1.55		1.56→1.9	1.9→2.0	2.4	4.9	528
	529	1.6	1.6		1.6→1.8	1.8→2.5			529
Shrinkage (vol. %)	525	7→6	6→5		3.5				
	526	5	6						
	527	12→9	(10)	15	6→0				
	528	8	8→5		5→0				
	529	7→5	5→4		4→0				
Vane shear strength (gm/cm^2)	525	50	30		50→>200				
	526		<50						
	527	<100	<100	800	150→>400				
	528	40	50→200	800	30→>300				
	529	50	50		50→>600				

Physical Properties of Lithologic Units (estimated averages)

65→56 = trend top → bottom of unit
55 = no trend visible
(10) = only few or one values

exist between these two types. Representative major element analysis by shore-based XRF, through collaboration with A. R. Duncan and D. L. Reid of the University of Cape Town, appear in Table 3. The analysis serves to illustrate some features of a probable overall trend in basalt composition from the ridge crest down into the adjacent ocean basin. The sample from ridge crest Site 525 is an aphyric basalt from a glassy pillow margin. It has the chemistry of a quartz tholeiite, with higher K_2O, TiO_2, P_2O_5, and FeO content than normally associated with a mid-ocean ridge basalt (MORB), consistent with considerable differentiation. The sample from the deepest Site 527 is a highly plagioclase phyric basalt from a flow interior. Its chemistry is that of an olivine tholeiite

Table 3. Representative XRF analyses of basalt samples from the Leg 74 Walvis transect.

	525A-59-4, 25 cm	527-41-4, 10 cm
SiO_2	50.20	48.82
TiO_2	2.49	1.17
Al_2O_3	13.95	16.91
Fe_2O_3	12.92	10.79
MnO	0.19	0.17
MgO	5.33	5.86
CaO	9.49	12.66
Na_2O	2.49	2.52
K_2O	1.03	0.17
P_2O_5	0.31	0.10
LOI	0.90	0.19
H_2O	0.51	0.93
Totals	99.82	100.29
Depth[a]	61	14

[a] Depth below top of basement in meters.

with K_2O, TiO_2, and P_2O_5 contents similar to those encountered in MORB, although higher FeO and lower MgO indicate a somewhat more evolved magma.

The major element chemistry of basalts from the Walvis Ridge crest resembles neither that of MORB previously recovered from the South Atlantic nor that of alkalic basalts on the spatially associated island of Tristan da Cunha. The Walvis Ridge has apparently been the locus of distinctive magma evolution.

PALEOMAGNETIC RESULTS

The results of the paleomagnetic measurements are included in Figures 4–7. The white, unlithified ooze of Pliocene to mid-Miocene age at all sites proved to be too weakly magnetized for measurement even with a superconducting rock magnetometer. The remaining Neogene material was contaminated by a strong viscous remanence acquired during sample handling that could not be reliably removed. Thus an analysis of paleomagnetic results for the HPC material is not reported, and detailed study was confined to undisturbed Paleogene rotary-drilled cores and especially to the lithified lower Paleocene to Cretaceous interval at Sites 525, 527, 528, and 529.

The latter proved to be quite stably magnetized, with median demagnetizing fields of 200–300 Oe and directional change of less than 20° over a 600-Oe coercive force range. We selected 43 pilot samples for detailed a.c. demagnetization in order to determine the optimum field for cleaning treatment of samples. The results show a record that is completely consistent with the type section at Gubbio, Italy (Alvarez et al., 1977). The Cretaceous/Tertiary boundary occurs near the top of the reversed interval between Magnetic Anomalies 29 and 30. The complete Paleocene-Cretaceous sequence of Anomalies 28–31 was recognized at all four sites, and Anomalies 25, 26, 27, and 32 are seen at some sites. Figure 9 shows a summary diagram together with the preferred time scale of Ness et al. (1980). The basement ages derived from these magnetic measurements indicate that at Site 525 the basement is of Anomaly 32N age; at 527, Anomaly 31N age; and at 528, Anomaly 31N. These

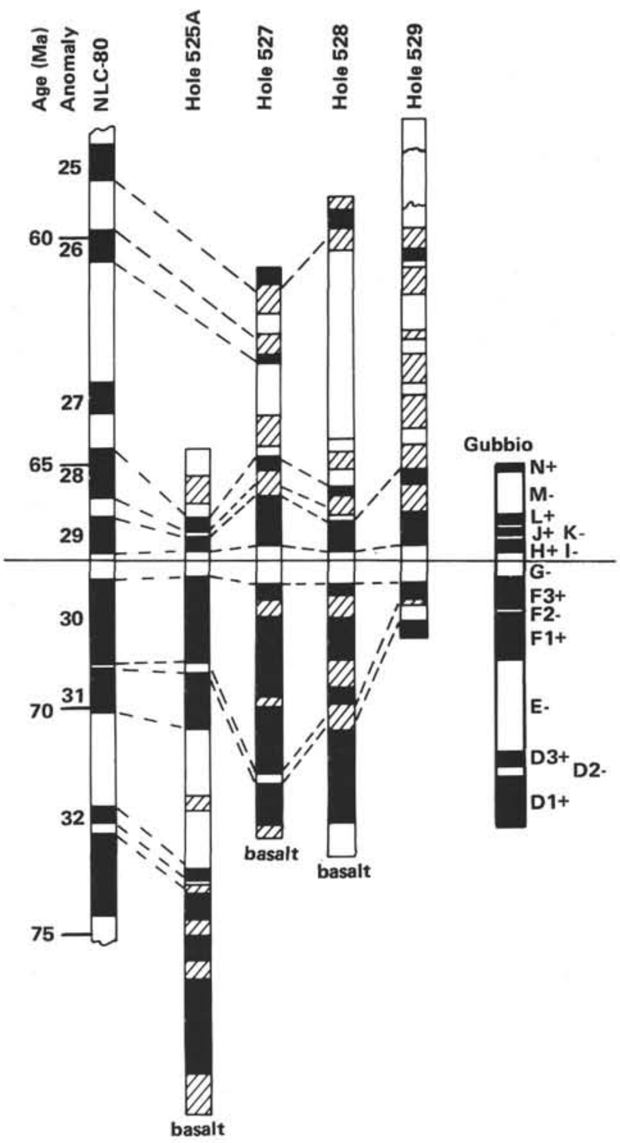

Figure 9. Summary diagram of Late Cretaceous–early Tertiary paleomagnetic results from four Leg 74 sites, using the time scale of Ness et al. (1980), with comparisons to the seafloor spreading anomaly pattern and the paleomagnetic measurements of the Gubbio section (Alvarez et al., 1977). Black intervals indicate normal polarity; white intervals, reversed polarity; and diagonal line intervals (Leg 74 sites) are areas of no recovery.

data are consistent with the biostratigraphic ages, the mapped crustal anomalies, and with the hypothesis that the Walvis Ridge was formed by seafloor spreading processes at a mid-ocean ridge.

SEDIMENTATION HISTORY

The sediments of the Walvis Ridge are dominated by biogenic carbonate. Only in the late Maestrichtian and early Paleocene are the sediments rich in volcanogenic material, apparently derived from active centers on the Ridge itself. This activity was particularly great during the latest Maestrichtian, dropped markedly in the early Paleocene, and disappeared from the record in younger times.

The degree of carbonate preservation and rates of sediment accumulation varied greatly through the Cenozoic. This is evidenced by changes in estimates of preservation of the calcareous assemblages and variation in the average carbonate accumulation rates in the study area (Fig. 10A, C).

The preservation of the calcareous faunas and floras generally parallels changes in the CCD. From the middle to late Eocene through the Oligocene, microfossils are generally poorly preserved; those of the late Oligocene to late Miocene are moderately well preserved, and those of the latest Miocene through Quaternary are well preserved. Preservation in the early Paleogene was poor to moderate, with diagenetic alteration in the thicker sections (shallower sites) having the greatest overall effect on the assemblages. Hiatuses are most common in the late Eocene through late Oligocene parts of the sites (Fig. 10B). In this interval they do not appear to have a clear depth dependency; breaks in the record are found at the deepest (527) and shallowest (525, 526) sites but not in between. However, this interval of abundant hiatuses has a lower accumulation rate, with poorer nannofossil preservation at all sites. The increased frequency of hiatuses in the mid-Paleogene is probably caused by a relatively high ratio of dissolution to supply. Hiatuses in the late Neogene occur at the mid-depth sites (528, 529).

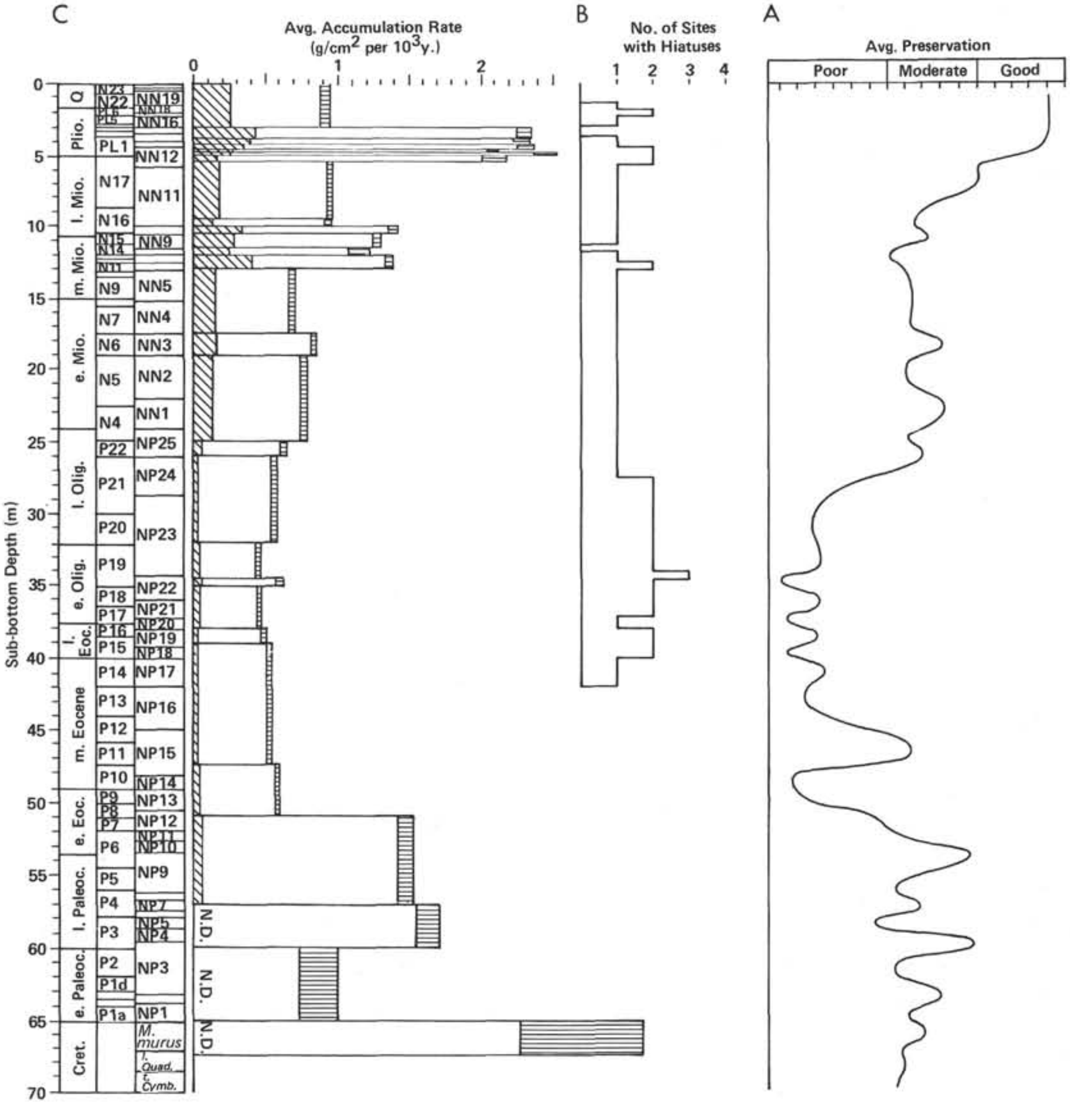

Figure 10. A. Average foraminifer preservation. B. Abundance of hiatuses. C. Average sediment accumulation rates for Leg 74 sites. Preservation is a subjective estimate. Each estimate is given a numerical code and averaged over all five sites. Hiatuses in the sections were considered present only when both calcareous nannofossils and foraminifers indicated that one or more biostratigraphic zones were not represented. Accumulation rates were calculated for three separate components: coarse-grained (>63 μm) material (dominated by foraminifers and indicated by diagonal shading); fine-grained carbonate (>63 μm, dominated by calcareous nannoplankton); and noncarbonate sediments (indicated by horizontal shading). Accumulation rates for each component were averaged over all intervals recovered. Both hiatuses and shallow-water sediments at Site 526 were excluded in the calculation of averages (Fig. 11). N.D. indicates lithified intervals where sediments could not be separated into size fractions.

Because they are closely associated with slump deposits and occur near points of peak accumulation (Fig. 10C), they are probably linked to slumping and erosion rather than to dissolution.

The record of average accumulation rates from sites in this region shows the same general features. Carbonate accumulation averaged about 1 $g/cm^2/10^3$ y. during much of Cenozoic. There are four maxima in average accumulation: (1) in the late Maestrichtian, when volcanic debris was an important sedimentary component and contributed nearly 1 $g/cm^2/10^3$ y. to the sediments; (2) in the late Paleocene to early Eocene, when no hiatuses occur; (3) in the latest mid-Miocene; and (4) in the earliest Pliocene. Of these four peaks, the one in the early Pliocene appears to be the largest. The two Neogene peaks occur at all five sites. Their presence in the shallowest site (526), where dissolution effects are thought to be negligible, suggests that these maxima result from increased carbonate productivity during the late middle Miocene and early Pliocene.

One of the chief purposes of drilling this suite of sites over a wide depth range was to investigate, in more detail than is generally feasible, the history of calcite dissolution in the water column. Figure 11 shows the estimated accumulation rates of sediment broken into three components: greater than 63 μm (almost entirely foraminifers), less than 63 μm (largely coccoliths), and the noncarbonate residue. It is apparent from this figure that the accumulation rate of foraminifers was generally highest at the shallowest site; we interpret the reduced accumulation of foraminifers at deeper sites as a measure of the loss by dissolution. The accumulation of fine-grained material was low at the shallowest sites, high at intermediate depths, and, during parts of the record, low again at the deepest sites. We interpret this as a result of winnowing, which preferentially inhibits the accumulation of fine material on the rises, and of dissolution, which has a significant impact on coccoliths only near the CCD.

The recovery of one exceptionally shallow section (Site 526) serves as a standard with no (or minimal) dissolution effects against which to compare the deeper sites. An interesting feature revealed by this comparison is that the degree of undersaturation with respect to calcite in the upper part of the water column (as indicated by Fig. 11) was considerably greater during periods of high carbonate accumulation (production). This suggests that the changes in dissolution rates extend to the shallower parts of the water column and are strongly linked to large-scale changes in productivity. If the carbonate dissolution rate at 2500 m water depth had been as high in the late Miocene and Oligocene (intervals of relatively slow carbonate accumulation) or during the mid-Miocene (intervals of rapid carbonate accumulation) as it was during the last 3 m.y., no foraminifers would have survived; instead we see that the Oligocene foraminiferal accumulation at 2500 m (Site 525) was not much less than at 1000 m (Site 526).

Figure 12 shows the magnitude of these dissolution effects for three time intervals. We divided the foraminifers into two fractions on a 150-μm sieve. In the Pleistocene, the accumulation of larger foraminifers is significantly affected by dissolution only at the deepest site, but the accumulation of smaller foraminifers is reduced by a factor of 2 between Sites 526 (1000 m) and 525 (2400 m), a surprising finding considering that the CCD was deeper than 4400 m throughout the interval. Coccolith accumulation, by contrast, was reduced by a factor of at

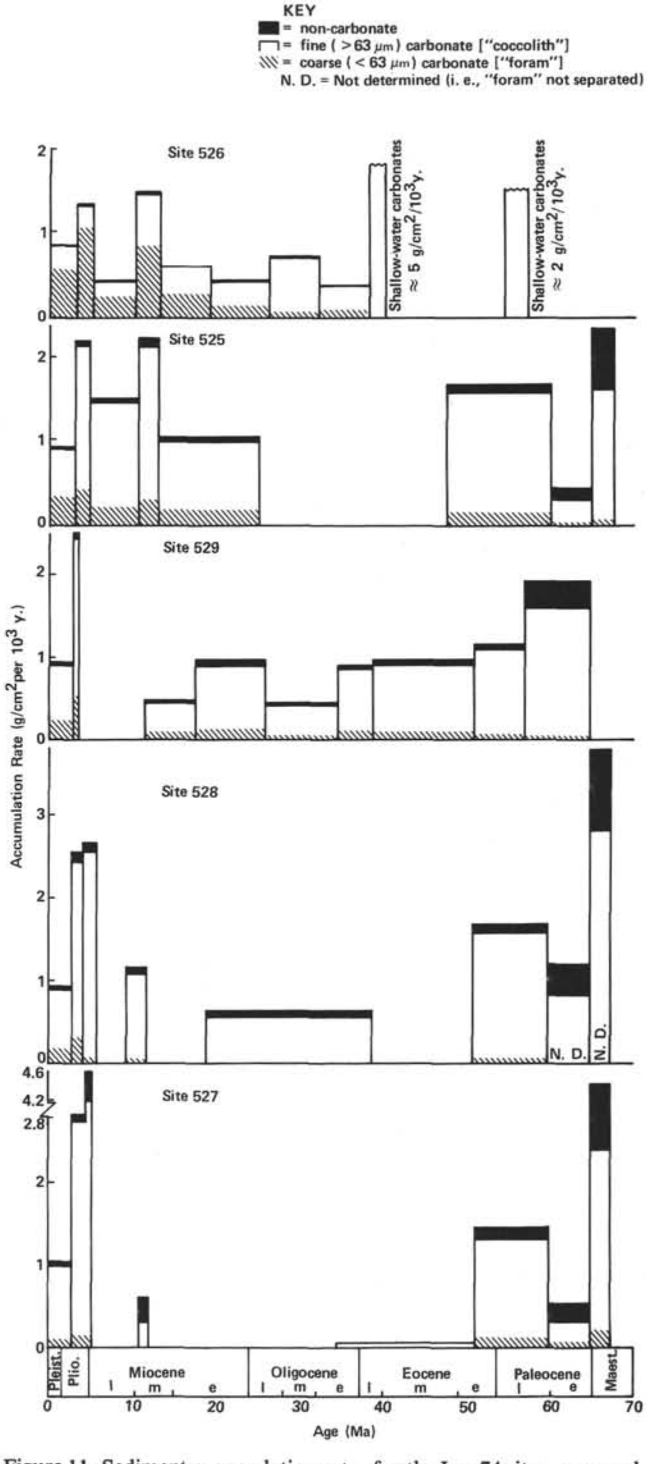

Figure 11. Sediment accumulation rates for the Leg 74 sites, arranged according to water depth from shallow (top) to deep (bottom). Shading and notation as in Figure 10.

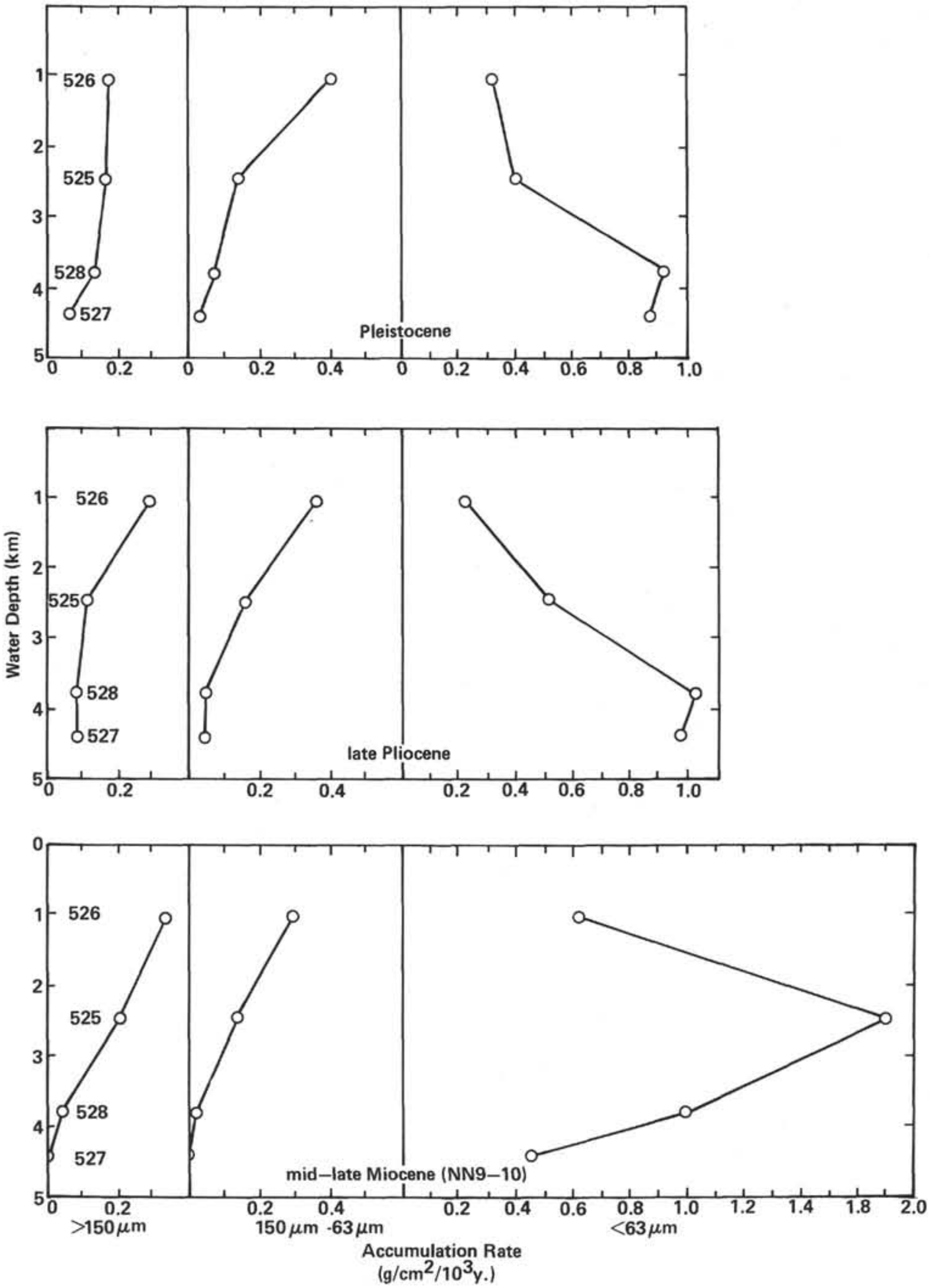

Figure 12. Average accumulation rates of three carbonate-size fractions (<150µm, 150–63µm, and <63µm) plotted as a function of depth during three time intervals. Data from Site 529 are excluded from these plots because slumping in the section gives anomalous accumulation rates.

least 3 at Site 526 as a result of winnowing (the factor is actually somewhat greater, since a significant accumulation of foraminifers smaller than 63 µm occurred at Site 526). In the late Pliocene, the pattern was somewhat similar to that of the Pleistocene, except that even the larger foraminiferal fraction is affected by dissolution at 2500 m.

We also show data from the mid–late Miocene (Zones NN9 and NN10), at which time the CCD was evidently not much deeper than the depth of Site 527. Much of the foraminiferal carbonate has been removed at Site 528, whereas at 527 foraminiferal accumulation is nil and the coccoliths noticeably reduced.

BIOSTRATIGRAPHY AND EVOLUTION OF WALVIS RIDGE FLORAS AND FAUNAS

Within the Leg 74 area, sedimentation commenced upon the Walvis Ridge in the early Maestrichtian (*Globotruncana tricarinata* foraminiferal zone or *Tetralithus trifidus* nannofossil zone). Sediments were deposited between the basalt layers. (Shallow-water faunas and apparent turbidites from shallow pinnacles contain *Inocer-*

amus, often in great abundance.) Both benthic faunas and the ratio of planktonic to benthic foraminifers in these sediments confirm the approximate depth of formation of basalts predicted by normal thermal subsidence models. Correlation of foraminiferal datums to paleomagnetics agrees with that in the Gubbio section (Alvarez et al., 1977). The first correlation of standard nannofossil zones to magnetics and foraminiferal datums was also possible at the Walvis Ridge sites.

Nannoplankton and planktonic foraminifers of the Maestrichtian are typical of middle latitudes. Preservation varies among the sites and appears to be strongly affected by the amount of sedimentary overburden. Nannofossils are moderately preserved throughout, but foraminifers are poorly preserved at the shallow Site 525 and intermediate Site 529; the best-preserved faunas are found at the deepest Site 527.

The Cretaceous/Tertiary boundary interval is included in four continuous sedimentary sequences and contains diverse nannofossil and foraminiferal biotas. Substantial volcanic material was added to sediments below the boundary at all sites—and into the Paleocene at Site 525. Just below the boundary there is a short zone of blue gray sediment containing a warmer-water foraminiferal fauna than in the deeper cores, implying the incursion of slightly warmer surface waters into this area just before the terminal Cretaceous event. All sediments are calcareous oozes with moderately well preserved nannofossils but not particularly well preserved foraminifers.

The input of volcanic materials in the basal Paleocene has altered the sediments to rich hues of brown and green at several sites. Fossils are nevertheless well preserved at all but Site 529, which is strongly lithified. The basal Tertiary *Globigerina eugubina* Zone was recovered, attesting to the relative stability of sedimentary conditions. Paleocene faunas are typical of middle latitudes, and floras contain temperate watermass indicators. The shallowest Site 526 probably lay close to sea level at this time and contained a carbonate shelf fauna. Sedimentation through the Paleocene appears to have been more continuous at the deeper than at the shallower sites, judging by the absence of several foraminiferal zones at Sites 525 and 529 near the end of the early Paleocene. However, no significant breaks were found in the nannofossil biostratigraphic sequence of the early Paleocene. Average accumulation rates (Figs. 10 and 11) were lower in the early Paleocene than in either the late Maestrichtian or late Paleocene. Some of the best-preserved nannofossils are found in the upper Paleocene at Site 529, despite the large overburden at this site. The Paleocene/Eocene boundary was easily recognized by the first appearance of the benthic foraminifer *Gavelinella beccariiformis* and by the first appearance of the calcareous nannofossil *Discoaster diastypus*.

Lower Eocene faunas are relatively well preserved at all sites, and benthic foraminifers indicate deposition at intermediate water depths. Planktonic faunas contain sufficient warmer-water elements to indicate warmed surface waters in this area. Subsequent preservation worsens markedly, and the South Atlantic episode of poorly preserved middle Eocene sediments is evidenced here on the Walvis Ridge. There are few well-preserved sequences from the middle into upper Eocene at any site. By the late Eocene Site 527 was approaching the paleo-CCD, and most foraminifers are dissolved. Nevertheless the nannoflora was useful for zonation in this interval. Little upper Eocene was recovered at any of the other sites. The faunas contain typical middle latitude species, and sediments are nearly all carbonate oozes. At this time the shallowest Site 526 lay near the shelf–slope transition; planktonic oozes contain large amounts of shallower-water sediments and fossils. The preservation of the calcareous nannofossils is poor through the Eocene interval; only large species are present.

The Eocene/Oligocene boundary is well preserved and appears continuous at Site 529, where a long transition zone containing moderately to well-preserved biotas was recovered. According to the calcareous nannofossil study, a very condensed interval containing the Eocene/Oligocene boundary is also present at Site 528. At the shallowest site (526) a regression and consequent sediment removal is indicated for this period.

The Oligocene faunas recovered at Site 529 included mainly temperate species, which are moderately well preserved, as well as several boreal types. *Chiasmolithus altus*, an Oligocene nannofossil species preferring cooler water masses, was also commonly found only at Site 526. A nearly complete section was found at the shallower Site 526, which, based on the presence of benthic uvigerinid faunas, must have lain at depths of 600–1000 m at this time. Shallow-water materials continue to be transported into this area, particularly during a middle Oligocene regression which is marked by increased sediment erosion at the shallower site and by the presence of bryozoan and mollusk debris and a *Uvigerina semivestita–U. mexicana* fauna. Other sites apparently lay too deep to demonstrate the effects of the regression. Site 527 lay below the CCD for foraminifers through this time. Only at Site 526 was an interval of abundant *Braarudosphaera* detected within the Oligocene.

The Oligocene/Miocene boundary was cored at four sites; only Site 527 lay below the CCD at this time. The boundary is based primarily on the last occurrence of the calcareous nannofossil species *Sphenolithus ciperoensis* and the *Turborotalia kugleri/Globigerinoides primordius* concurrent ranges. Foraminifers and nannofossils were moderately well preserved except adjacent to hiatuses. Benthic foraminifers indicated that sediments were nearly all from intermediate depths, except at Site 527, which contained red clays with no foraminifers and few nannofossils.

It is difficult to use foraminifers to zone the upper lower to middle Miocene intervals because of the lack of tropical index fossils. The nannofossils are generally amenable to a tropical zonation. The buildup of the Antarctic ice sheet coincident with the NN5/NN6 zonal boundary is evidenced by a large influx of keeled globorotalids and forms of *Globigerinoides*, suggesting increased density stratification of the eastern margin of the South Atlantic gyre.

Carbonate oozes of late Miocene age contained middle latitude and temperate water floras and faunas; the sections were relatively complete and preservation moderate. A change in benthic foraminifers at the end of the Miocene may correlate with the high productivity episode of the post-Messinian time in the Atlantic.

Three very well preserved and supposedly complete Pliocene sections containing boreal and temperate planktonic fossils were recovered from this area. A marked decrease in boreal fossils and their replacement by a typical middle latitude fauna is indicated in all the mid-Pliocene faunas coincident within the extrapolated base of the Gauss. The CCD sank below the deepest site (527) near the base of the Pliocene; thus this site also contains fossils that are sufficiently well preserved for detailed climatic studies. This site is on the northwestern end of the transect (Fig. 1). That it may have lain under a slightly different surface watermass in the Pliocene is demonstrated not only by differing planktonic foraminiferal faunas but also by a different sequence of changes in these faunas through the Pliocene. A Pliocene section was recovered at Site 529, but active slumping had disturbed the upper Miocene sequence. The upper Pliocene section accumulated at slower rates and is consistently thin at all sites drilled.

Portions of the early to late Pleistocene contained well-preserved temperate floras and faunas in coarse-grained foraminiferal nannofossil oozes. Slumping of Pliocene into lower Pleistocene sediments occurred at Site 529.

CONCLUSIONS

1. As suggested by crustal magnetic anomaly patterns, the section of the Walvis Ridge under study was formed at a mid-ocean ridge spreading center. The age of the basement rocks is approximately 69–71 m.y. (Magnetic Anomaly 31 to 32 time), with the deeper sites slightly younger than those upslope.

2. The basement is composed of basaltic pillows and flows intercalated with nannofossil chalks and limestones containing a significant volcanogenic component. The major element chemistry shows a change from quartz tholeiitic basalt at the ridge crest to olivine tholeiitic basalt down the northwestern flank. The chemistry of crestal magmas differs from that of mid-ocean ridge basalt previously recovered from the South Atlantic.

3. The lithology of the sections is dominated by carbonate oozes and chalks. Dissolution is seen to have had a marked effect on accumulation in the deeper sites, particularly in the upper Miocene, Oligocene, and middle to upper Eocene.

4. Volcanogenic material is common in the Maestrichtian and lower Paleocene and is probably derived from sources on or near the Walvis Ridge.

5. Average accumulation rates suggest that there were three peaks in the rate of supply of carbonate to the seafloor: one during the early Pliocene, one in the late middle Miocene, and one in the late Paleocene to early Eocene. During much of the rest of the Cenozoic, carbonate accumulation averaged 1 $g/cm^2/10^3$ y.

6. The rates of dissolution as a function of depth can be calculated by using data from all the sites in the transect. Initial results of such an analysis indicate that the upper part of the water column showed a greater degree of undersaturation with respect to carbonate during times of high carbonate accumulation (production). Even when the CCD was below 4400 m, a large amount of carbonate was dissolved in the upper part of the water column. This may render the "lysocline" and "R_0 level" concepts of Berger (1977) inapplicable for at least some parts of the record.

7. The effects of winnowing are shown by a systematic downslope increase in the clay (noncarbonate fraction) and coccolith (<63 μm size fraction) accumulation rates. The coccolith accumulation rate is lowered at the deeper sites only during intervals of intense dissolution.

8. Standard zonations from the foraminifers and calcareous nannofossils could be used through much of the section; however, many of the foraminiferal species commonly used in tropical zonations are absent in this area, and in some cases the ranges of species appear to be diachronous through latitude. Foraminiferal datums and standard nannofossil zones of the Maestrichtian are correlated to paleomagnetics for the first time.

9. The faunas and floras of the Walvis Ridge sites are temperate in nature. An indication of warmer faunas is found in the uppermost Maestrichtian and lower Eocene and of cooler faunas in the Oligocene, middle Miocene, and lower Pliocene. The boreal elements of the lower Pliocene faunas are replaced by more temperate forms in the mid-Pliocene.

10. The Cretaceous/Tertiary boundary was well recovered in four of the five sites drilled, and sediments contain well-preserved nannofossils but poorly preserved foraminifers. The basal Tertiary *Globigerina eugubina* Zone was recovered consistently but was poorly preserved.

11. The shallowest site (526) did not sink below sea level until the late Paleocene. Here, benthic faunas are distinctly different from those at deeper sites and at sites on continental slopes at similar depths.

12. At Site 526, the effect of a middle Oligocene regression is recorded by the benthic foraminifers, which indicate a rapid shoaling followed by a deepening. Other sites were deep enough so that no change was noted in the benthic fauna.

EXPLANATORY NOTES

Responsibilities of Authorship

The site chapters are authored by the entire scientific party; ultimate responsibility for content lies with the co-chief scientists. These chapters are organized as follows (authors' names are in parentheses).

Site Data (Moore, Rabinowitz)
Principal Results (Moore, Rabinowitz)
Background and Objectives (Rabinowitz, Moore)
Operations (Rabinowitz)
Sediment Lithology (Borella, Duée, Fütterer, Lever, O'Connell)
Inorganic Geochemistry (Borella)
X-Ray Diffraction Analysis (Lever, Borella)
Biostratigraphy (Boersma, Jiang, Manivit)
Sediment Accumulation Rates (Shackleton)

Igneous Petrology (Richardson, O'Connell)
Magnetics (Chave, O'Connell)
Physical Properties (Kleinert)
Downhold Measurements (Rabinowitz)
Summary and Conclusions (Moore, Rabinowitz)

The interpretations of individual authors have been retained in the sections for which they were responsible. As a result, there is sometimes a conflict in interpretation between a particular section and the Conclusions.

NUMBERING OF SITES, HOLES, CORES, AND SAMPLES

DSDP drill sites are numbered consecutively beginning with the first site drilled by *Glomar Challenger* in 1968. Site numbers are slightly different from hole numbers. A site number refers to one or more holes drilled while the ship was positioned over one acoustic beacon. These holes may be located within a radius as great as 900 m from the beacon. Several holes may be drilled at a single site by pulling the drill pipe above the seafloor (out of one hole) and moving the ship 100 m or more to begin drilling another hole.

The first (or only) hole drilled at a site takes the site number. A letter suffix distinguishes each additional hole at the same site. For example, the first hole takes only the site number, the second takes the site number with suffix A, the third takes the site number with suffix B, and so forth. It is important, for sampling purposes, to distinguish among the holes drilled at a site, since sediments or rocks recovered from different holes usually do not come from identical positions in the stratigraphic column.

The cored interval is measured in meters below the seafloor. The depth interval of an individual core is the distance between the point below seafloor that the coring operation began and the point at which it ended. Each coring interval is generally 9.5 m long, which is the nominal length of a core barrel; however, the coring interval may be shorter or, sometimes, slightly longer. "Cored intervals" are not necessarily adjacent to each other, but may be separated by "drilled intervals." In soft sediment, the drill string can be "washed ahead" with the core barrel in place, but not recovering sediment, by pumping water down the pipe at high pressure to wash the sediment out of the way of the bit and up into the space between the drill pipe and wall of the hole. However, if thin, hard-rock layers are present, it is possible to get "spotty" sampling of these resistant layers within the washed interval and thus have a cored interval greater than 9.5 m.

Cores are numbered serially from the top of the hole downward. Core numbers and their associated cored interval in meters below the seafloor are normally unique for a single hole, unless an interval is cored twice. When this occurs, the core number is assigned the suffix "S," for "supplementary."[6]

Full recovery for a single core is normally 9.28 m of sediment or rock, which is in a plastic liner (6.6-cm ID), plus about a 0.2-m-long sample (without a plastic liner) in the core catcher. The core catcher is a device at the bottom of the core barrel which prevents the cored sample from sliding out as the barrel is being retrieved from the hole. After retrieval the core is cut into 1.5-m-long sections that are numbered serially from the top of the core (Fig. 13). When there is full recovery, the sections are numbered from 1 through 7, with the last section shorter than 1.5 m.

When the core liner is recovered full to the top, the core is still cut into six 1.5-m sections, measured from the bottom of the liner, and the extra 0.28-m section at the top is designated Section 0, or the "zero section." The zero section is ignored in calculations of depth below the seafloor.

When there is partial recovery, the original stratigraphic position of the material in the cored interval is unknown. If the recovered material is contiguous we assign the top of it to the top of the cored interval and number sections serially from the top, beginning with Section 1 (Fig. 13).[7] There are as many sections as are needed to accommodate the material. For example, 4 m of material are divided into 3 sections—2 upper sections 1.5 m long and a final lower section only 1.0 m in length. If the shipboard scientists determine that material recovered is not contiguous, then sections are divided and numbered serially, as with contiguous material, and gaps labeled as voids for sediments (Fig. 13) or marked by spacers for igneous rocks (see Igneous Rocks section).

Samples are designated by centimeter distances from the top of each section to the top and bottom of the sample in that section. A full identification number for a sample consists of the following information: leg, site, hole, core number, and interval (in centimeters from the top of section). For example, a sample identification number of 74-525A-3-3, 12–14 cm is interpreted as follows: 12–14 cm designates a sample taken at 12–14 cm from the top of Section 3 of Core 3 from the second hole drilled at Site 525 during Leg 74. A sample from the core catcher of this core is designated as 74-525A-3,CC.

When making a sample request, please refer to a specific interval within a section of a core. DSDP now has sample listings from each leg listed on microfiche cards with assigned absolute sample depths in meters. For requests, please write to the DSDP Information Handling Group.

Handling of Cores

A core was normally cut into 1.5-m sections, sealed, and labeled, then brought into the core laboratory for processing. Long core spinner magnetism measurements, gas analyses, thermal conductivity measurements, and continuous wet-bulk density determinations using the Gamma Ray Attenuation Porosity Evaluator (GRAPE) were made before splitting sections.

The cores were then split longitudinally into "working" and "archive" halves. Samples were taken from

[6] Note that this designation has been used on previous legs as a prefix to the core number for sidewall core samples.

[7] This technique differs from the labeling systems used on Legs 1 through 45, which designated a "zero section" but did not have a "number 7 section."

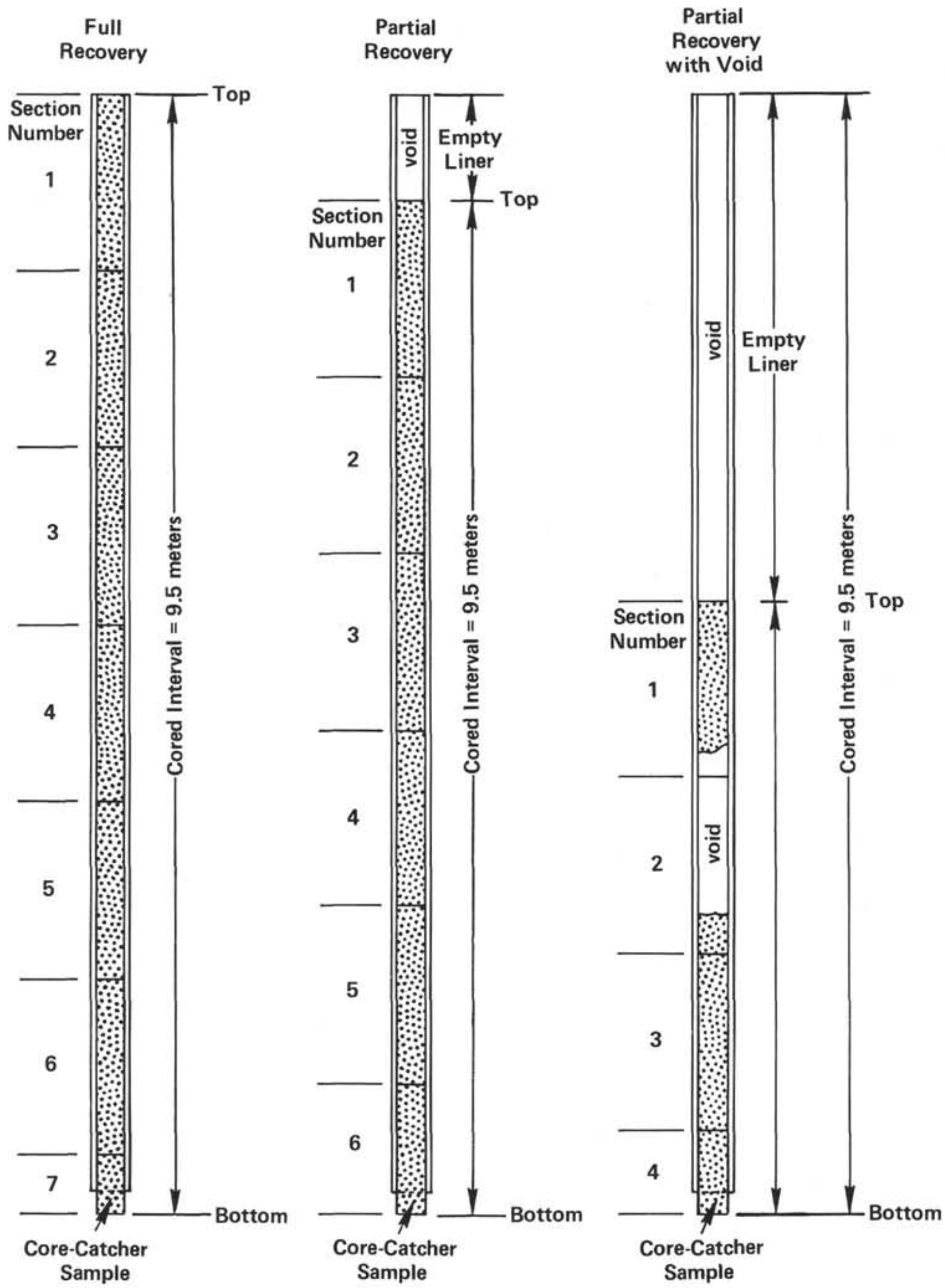

Figure 13. Diagram showing procedure in cutting and labeling of core sections.

the "working" half, including those for determination of grain-size distribution, mineralogy by X-ray diffraction, sonic velocity by the Hamilton Frame method, wet-bulk density by a static GRAPE technique, water content by gravimetric analysis, carbon–carbonate analysis, calcium carbonate percentage (Carbonate Bomb), geochemical analysis, paleontological studies, and others.

Smear slides (thin sections for lithified sedimentary and igneous rocks) from each major lithology, and most minor lithologies, were prepared and examined microscopically. The archive half was then described and photographed. Physical disturbance by the drill bit, color, texture, structures, and composition of the various lithologies were noted on standard core description forms. All prime data are routinely microfilmed and some are digitized for computer retrieval.

After the cores were sampled and described, they were maintained in cold storage aboard *Glomar Challenger* until they could be transferred to the DSDP repository. Core sections of sediments removed for organic geochemistry study were frozen immediately on board ship and kept frozen. All Leg 74 cores and frozen cores are presently stored at the DSDP West Coast Repository (Scripps Institution of Oceanography).

When the cores arrive at the repository, all hydraulic piston cores are routinely photographed on 35-mm continuous flow microfilm. These films will be made available at the termination of the one-year proprietary hold.

Hydraulic Piston Corer (HPC)

On Leg 74 the Serocki-Storms-Cameron Hydraulic Piston Corer (HPC) was used successfully to recover undisturbed sediments at Holes 525B, 526A, 526B, and 528A. Recovery averaged 82%; if we eliminate Hole 526A, recovery averaged a remarkable 100%. HPC holes are designated in the same way as rotary-drilled holes.

The principles of the operation of the hydraulic piston corer are presented in Figure 14. The hydraulic piston corer is located within the lowermost part of the drill string and is flush with the base of the drill bit before it is fired. Once fired, the cores ideally penetrate 4.4 m into the underlying sediment. The full extension of the HPC to this length is reflected on the rig floor by complete pressure bleed-off following the shot. After penetration, the HPC is pulled up 4.4 m to a position within the lowermost part of the drill string. The whole drill string is then raised to a point where a drill string tool joint appears at the level of the rig floor. The raised interval ranges from 0.0–9.5 m (length of one joint of drill pipe). Thus a total open hole beneath the drill bit can be as high as 9.5 m + 4.4 m, or 13.9 meters. The drill string is then separated at the tool joint, and the inner core barrel with the 4.4 m of sediment is pulled to the rig floor on the sandline.

After removal of the core, the HPC inner core barrel is reloaded and returned to the base of the drill string. The HPC drill bit then washes down through the sediment interval just cored, but only for a distance of approximately 3.4 m. The last meter of lowering is done without washing. At that point the base of the drill string is at the desired level for the next HPC shot.

The presence of an open hole below the drill string during the time the HPC inner core barrel is retrieved and reloaded and the fact that the drill string washes down 3.4 m and is pushed the last meter begin to explain why the upper parts of many of the hydraulic piston cores are contaminated with material previously cored and disturbed. The raising of the entire drill string as much as 9.5 m also explains why a mud line core may be taken twice.

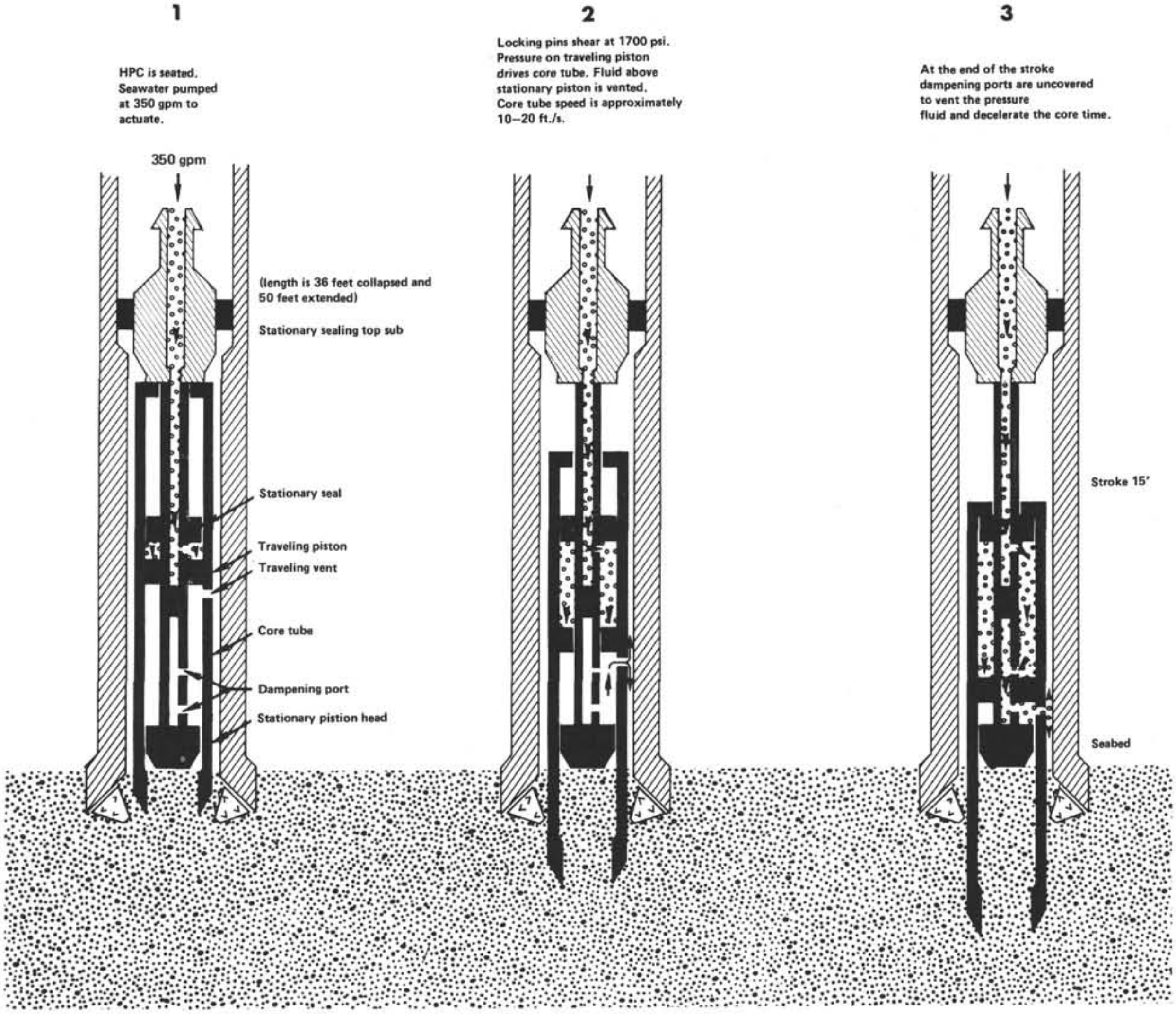

Figure 14. Operational sequence, DSDP hydraulic piston corer.

Sediments and Sedimentary Rocks

Core Description

Drilling Disturbance

Recovered rocks, and particularly the soft sediments, may be extremely disturbed mechanically. This disturbance is the result of the coring technique, which uses a large (25-cm diameter) bit with a small (6.0-cm diameter) opening for the core sample. The following disturbance categories are used for soft and firm sediment:

1) Slightly deformed: bedding contacts are slightly bent.

2) Moderately deformed: bedding contacts have undergone extreme bowing. Firm sediment is fractured.

3) Very deformed: bedding is completely disturbed or homogenized by drilling, sometimes showing symmetrical, diapir-like structure. Firm zones may have relic "drill biscuits" in a breccia or homogeneous matrix.

4) Soupy: water-saturated intervals which have lost all aspects of original bedding.

These categories are coded on the core description form in the column headed "Drilling Disturbance" (Fig. 15).

Sedimentary Structures

In the soft, and even in some harder, sedimentary cores, it may be extremely difficult to distinguish between natural structures and structures created by the coring process. Thus the description of sedimentary structures was optional. Locations and types of these structures appear as graphic symbols in the column headed "Sedimentary Structures" on the standard core description form (Fig. 15) and the expanded hydraulic piston core description form (Fig. 16). Figures 17 and 18 give the keys to these symbols.

Where distinguishable, bioturbation is noted in the graphic column. A summary of the most common biogenic sedimentary structures (ichnofossils) observed in DSDP cores is given in Figure 19.

Color

Colors of the geologic material are determined with a Munsell or Geological Society of America Rock Color Chart. Colors were determined immediately after the cores were split and still wet.

Lithology

The graphic column presented on the core description form is based on the lithologies and represented by a single pattern or by a grouping of two or more symbols. The symbols in a grouping correspond to end-members of sediment constituents, such as clay or nannofossil ooze. The symbol for the terrigenous constituent appears on the right-hand size of the column, the symbol for the biogenic constituent(s) on the left-hand side. The abundance percentage of any component is in approximately equal proportion to the width of the graphic column its symbol occupies. For example, if the left 20% of the column has a diatom ooze symbol and the right 80% a silty-clay symbol, the sediment contains 20% diatoms and 80% mud.

Because of the difference in the length-to-width ratio between the actual sediment core and the graphic lithologic column, it is not possible to reproduce structures as they appeared in the core; they would appear highly flattened and otherwise distorted. The same is true for rock fragments or pebbles in the cores. Therefore the locations of pebbles are shown by a solid square and the depth of small "patches" of ash or other lithologic changes are shown by a triangular inset of the appropriate lithologic symbol on the right side of the lithologic column (Fig. 18). This convention applies only to lithologies which do not extend across the entire core.

Format, style, and terminology of the descriptive portion of the core description forms (Figs. 15 and 16) are not controlled by the "Mandatory Graphic Lithologic Column Scheme" beyond the minimal name assignment derived from the lithologic classification (described in the following section). Colors and such additional information as structures and texture are included in the text portion of the core description.

Smear slide (or thin section) compositions, carbonate content (% $CaCO_3$), and organic carbon content determined aboard ship are listed below the core description on these forms, where two numbers separated by a hyphen refer to the section and centimeter interval, respectively, of the sample. The locations of these samples in the core and a key to the codes used to identify these samples are given in the column headed "Samples" (Fig. 15). Locations and intervals of organic geochemistry (OG) and interstitial water (IW) samples are given in the graphic lithology column.

Lithologic Classification of Sediments

The basic classification system used here was devised by the JOIDES Panel on Sedimentary Petrology and Physical Properties (SPPP) and adopted for use by the JOIDES Planning Committee in March 1974. For the sake of continuity the Leg 74 shipboard scientists have used this basic classification with some minor modification, which we will point out when those topics are discussed. The general classification (which embraces several lithologies not encountered during Leg 74) is outlined in the following section. This classification is descriptive rather than genetic, and divisions between different types of sediment are somewhat arbitrary. We treat lithologic types not covered in this classification as a separate category termed "Special Rock Types."

The sediments recovered on Leg 74 are composed of calcareous biogenic components and terrigenous and pyroclastic sediments (Special Rock Types—Fig. 18).

Conventions and Descriptive Data

Composition and Texture

In this classification, composition and texture are the only criteria used to define the type of sediment or sedimentary rock. Composition is most important for describing sediments deposited in the open ocean, whereas texture becomes significant for hemipelagic and nearshore sediments. These data come principally from visual estimates of smear slides using a petrographic micro-

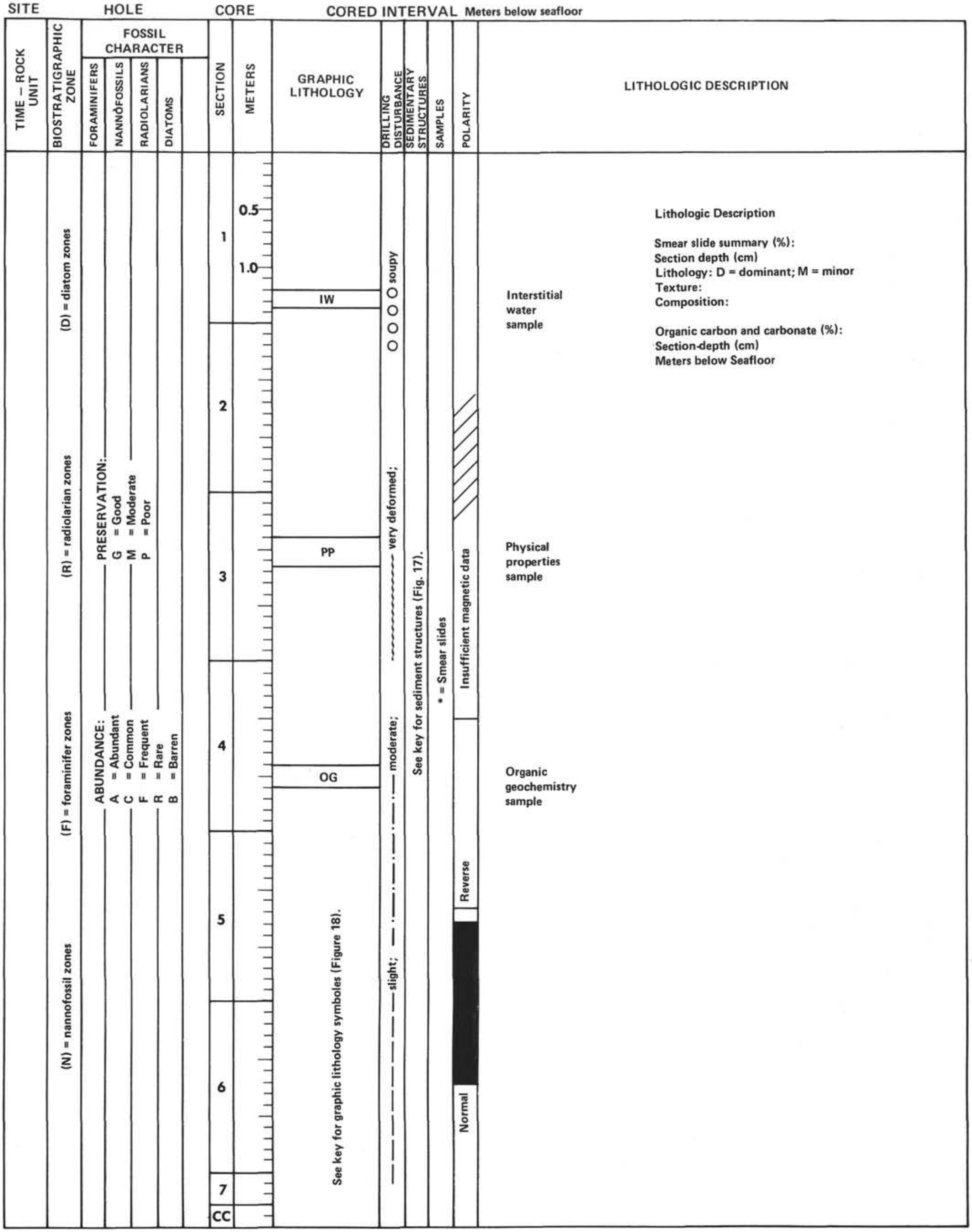

Figure 15. Sample core form (sediment).

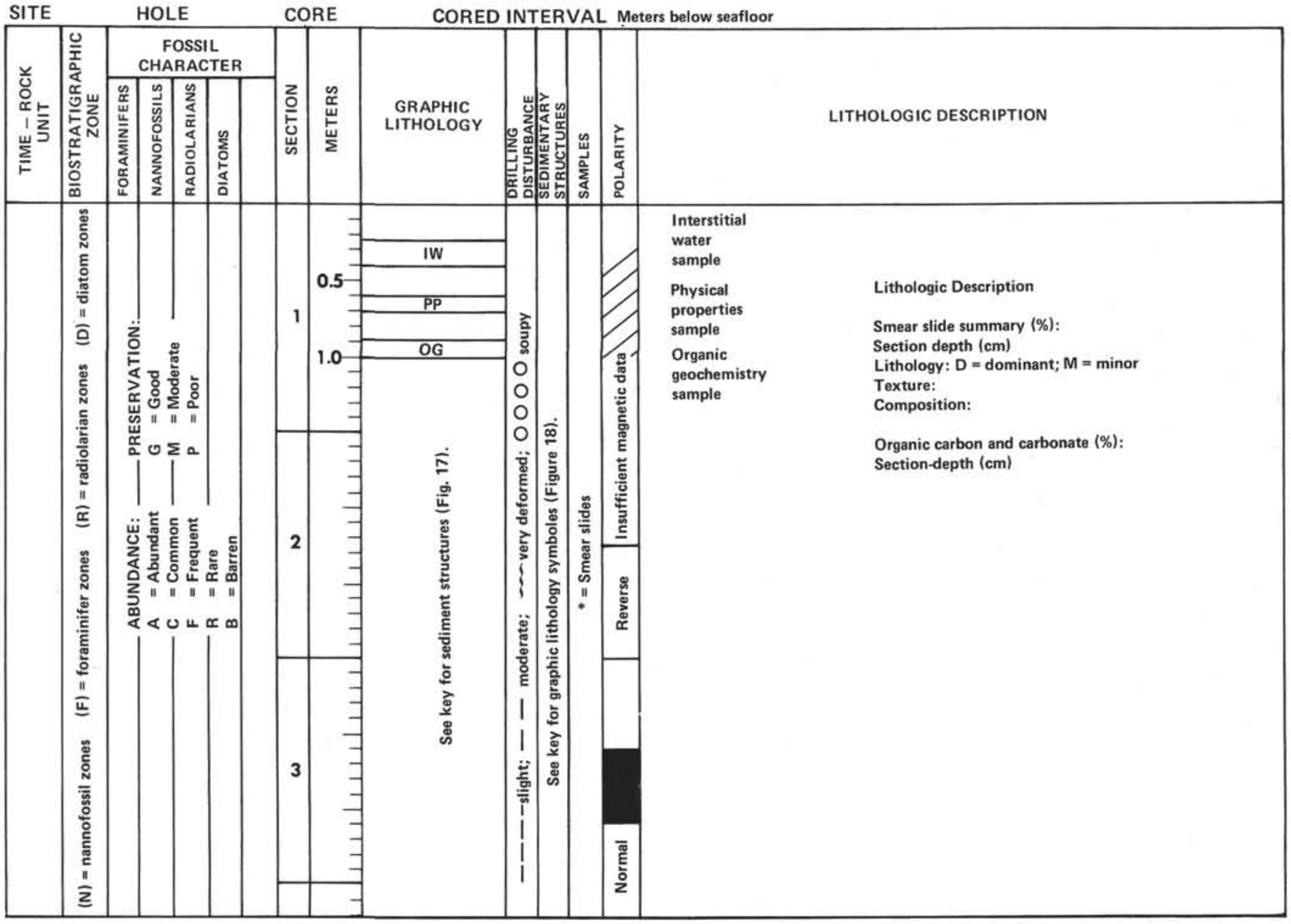

Figure 16. Sample core form (HPC).

scope. They are estimates of areal abundance and size components on the slide and may differ somewhat from more accurate analyses of grain size, carbonate content, and mineralogy (see Special Studies section). From past experience, we know that quantitative estimates of distinctive minor components are accurate to within 1–2%, but for major constituents accuracy is poorer (±10%). All smear slide estimates were done on board. Carbonate content is difficult to estimate from smear slides. Therefore, for many cores we determined the percentage of carbonate using the "Carbonate Bomb" technique of Müller and Gastner (1971). This method involves treating a powdered sample with HCl in a closed cylinder. The resulting pressure of CO_2 is proportional to the carbonate ($CaCO_3$) content of the sample, and this value is converted to percent $CaCO_3$ using the calibration factor of the manometer. The accuracy of this method is ±5%. Carbonate content determined in this manner is listed on the core description forms below the lithologic description.

Textures of sediments estimated from smear slides and listed as percent sand-silt-clay in the smear slide summary on the core description forms include all constituents. Thus, a diatomaceous ooze will have a greater percentage of silt-sized particles than a nannofossil ooze because of the different sizes of the tests of the two planktonic groups. This convention causes some confusion when naming terrigenous sediments that contain a significant number of microfossils. For example, a diatomaceous silty clay may have fewer silt-sized terrigenous particles (e.g., quartz and feldspar) than a nannofossil silty clay simply because many diatoms are silt-sized and are included as such in the textural estimate. To minimize this effect, we have chosen fairly broad compositional class boundaries (see the following) for mixed terrigenous and biogenic sediments. For this reason we preferred to replace clayey-silt or silty-clay terms by "mud" when used with a biogenic modifier.

Where applicable we used one or several modifiers in naming the type of sediment encountered. In all cases the dominant component appears last in the name, and minor components precede, with the least common constituent listed first. If minor constituents occur in amounts less than 10% they are not included in the name. This convention also holds for zeolites, Fe- and Mn-micronodules, and other indicators of very slow rates of sedimentation or nondeposition such as fish bones. Often these minerals are conspicuous even though greatly diluted. If deemed important and environmentally significant, as were nontronite, montmo-

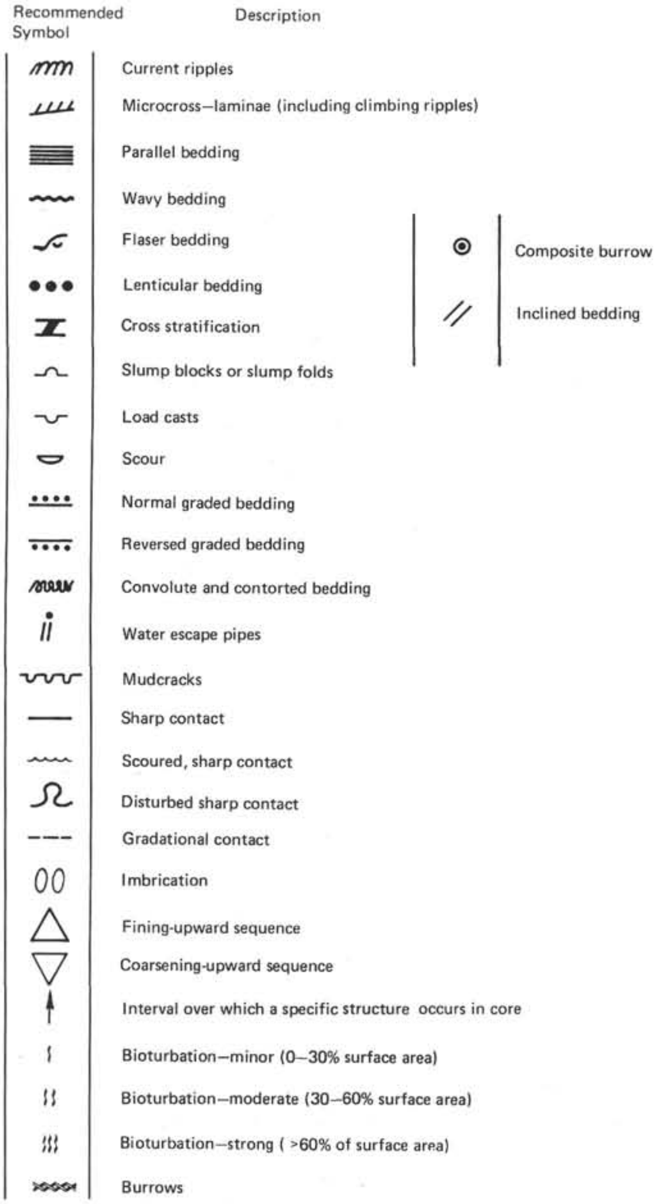

Figure 17. Symbols of sedimentary structures used on core description forms (sediment).

rillonite, and smectite on Leg 74, they are sometimes included in the name of the sediment or mentioned in the lithologic description.

Induration of Sediments

We recognize three classes of induration or lithification for calcareous sediments and sedimentary rocks in which the carbonate content is greater than 50% and only two classes for all other lithologic types.

1) Calcareous sediment and sedimentary rocks (categories after Gealy et al., 1971.)
   a) Soft = ooze; has little strength and is readily deformed under pressure of finger or broad blake of spatula.
   b) Firm = chalk; partially lithified and readily scratched with fingernail or edge of spatula.
   c) Hard = limestone; dolostone; well lithified and cemented; resistant or impervious to fingernail or edge of spatula.
2) Siliceous sediments (silica >50%)
   a) Soft = ooze; readily deformed by finger or broad blade of spatula.
   b) Hard = radiolarite, diatomite, chert, or porcellanite; core must be cut with band saw or diamond saw.
3) Terrigenous sediments (terrigenous components >50%).
   a) Soft = sand, silt, clay (or combinations of these); readily deformed by finger or broad blade of spatula.
   b) Hard = sandstone, siltstone, claystone, etc. (i.e., suffix *stone* added); core must be cut with band saw or diamond saw.

Types of Sediments and Compositional Class Boundaries

We distinguish five basic types of sediment: siliceous biogenic sediments, calcareous biogenic sediments, terrigenous sediments, volcanogenic sediments, and pyroclastic and hemipelagic sediments. Each type of sediment is discussed briefly in the following sections. An additional category, Special Sediment and Sedimentary Rock Types, which was used extensively on Leg 74, is also included.

Siliceous Biogenic Sediments

These are sediments in which biogenic silica or authigenic silica (opal CT and/or quartz) comprise at least 30% of the sediment. If the siliceous component is between 30 and 60%, the terrigenous (mud), calcareous biogenic, or volcanogenic modifier is retained. For example, "Muddy Diatomaceous Ooze" describes a soft sediment with at least 10% clayey silt and between 50 and 90% diatoms. If the siliceous component is >60%, the modifier(s) is dropped. A radiolarian ooze would have <10% clay or carbonate and >60% radiolarians. If the siliceous biogenic component is between 30 and 60%, the names for terrigenous or calcareous biogenic sediments or pyroclastic rocks apply, with the dominant siliceous constituent as a qualifier. Silica in amounts <10% is not acknowledged in the name.

Siliceous microfossils are often absent from hard siliceous rocks. If they have been dissolved and replaced by opal CT and/or quartz and these minerals make up >50% of the rock, the terms *porcellanite* and *chert* apply, defined as follows:

chert—a hard, conchoidally fracturing, varicolored sedimentary rock with semivitreous, vitreous, or waxy luster and conconsisting dominantly of silica.

porcellanite—a siliceous sedimentary rock with a dull or matte luster resembling that of unglazed porcelain. It is less hard, dense, and vitreous than chert and commonly has a lower silica content.

These definitions differ from conventional DSDP usage in that chert and porcellanite are textural terms independent of the silica polymorph (see Leg 63 ICD). If two

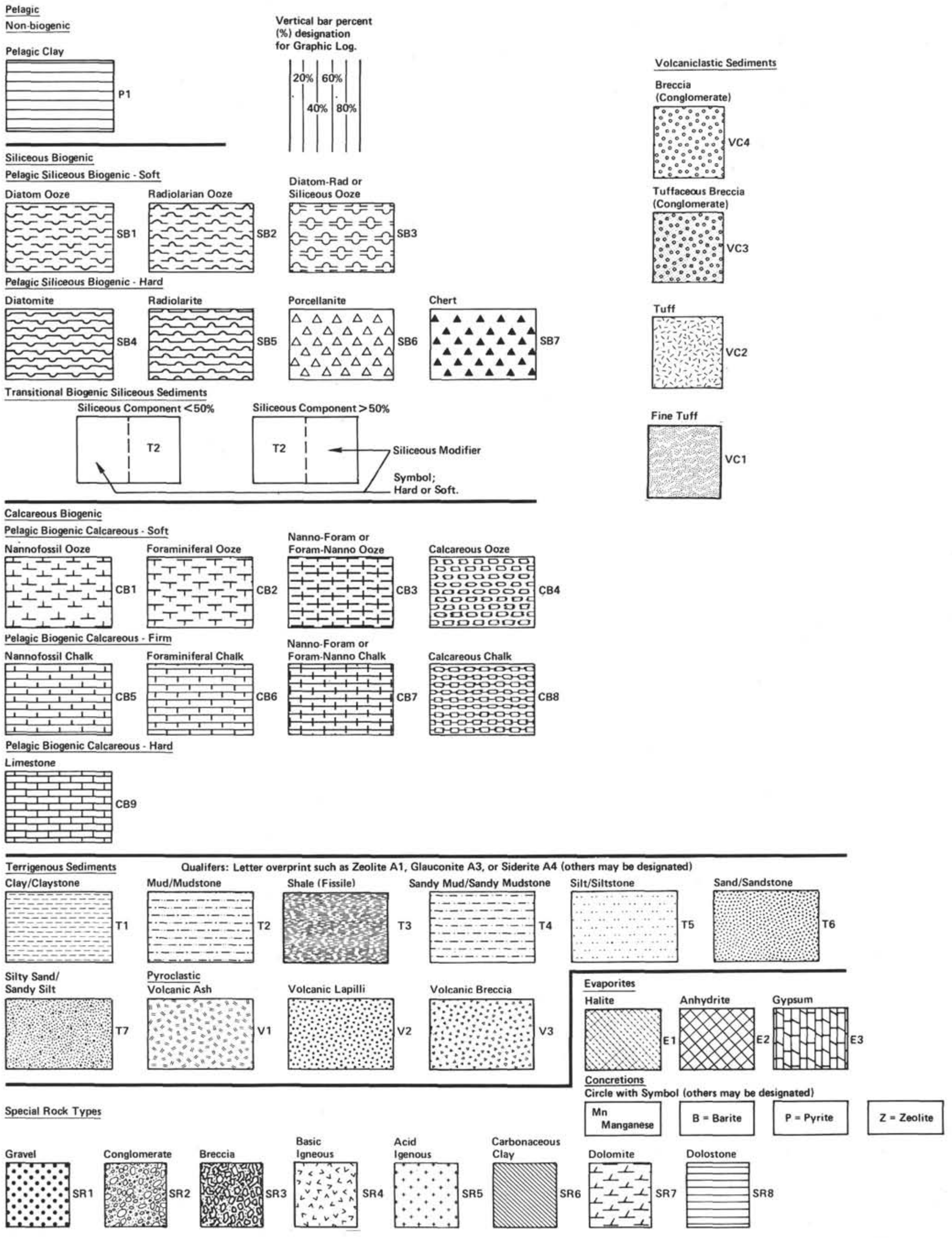

Figure 18. Graphic symbols to accompany the lithologic classification scheme.

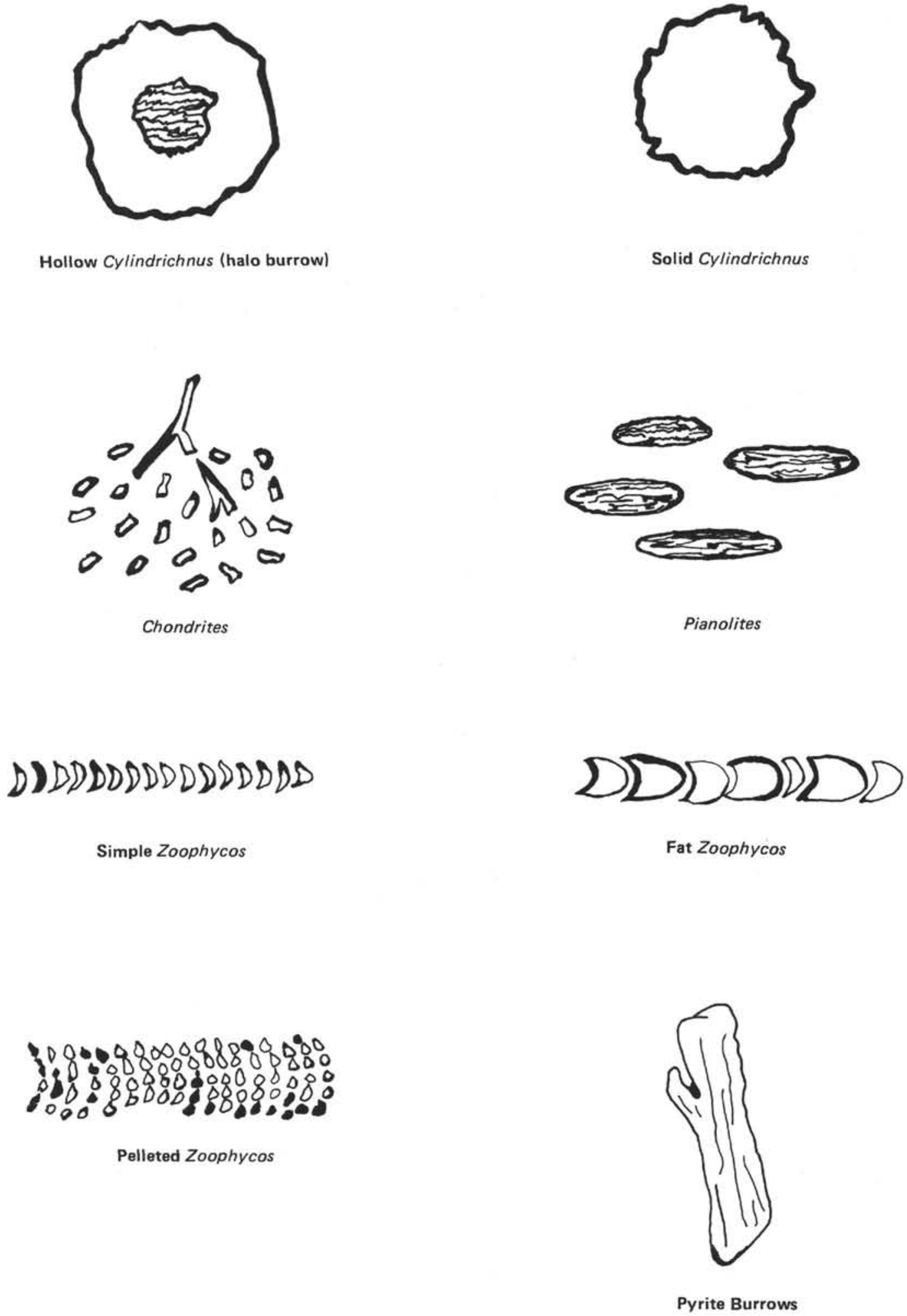

Figure 19. Trace fossils most common in DSDP cores.

modifers are used, their order is dependent on the dominant fossil type, the dominant component being listed last.

Calcareous Biogenic Sediments

These are sediments in which biogenic carbonate or carbonate of indeterminate origin (cement or recrystallized carbonate) comprises at least 30% of the sediment. If the carbonate component is between 30 and 60%, the terrigenous, siliceous biogenic, or volcanogenic modifiers are retained. For example, "Muddy Nannofossil Ooze" describes a soft sediment with at least 10% clay and between 30 and 60% calcareous nannofossils. If the calcareous component is >60%, the modifers are dropped. A nannofossil ooze would have < 10% clay or silica and 60% calcareous nannofossils. If the calcareous biogenic component is between 30 and 60%, the names for terrigenous or siliceous biogenic sediments or pyroclastic rocks apply, with the dominant calcareous constituent as a qualifier. Carbonate < 10% is not acknowledged in the name.

For firm and hard calcareous rock with carbonate contents > 50%, the terms *chalk, limestone*, and *dolostone*, apply. If the carbonate content is between 30 and 60%, the terrigenous modifier is retained. The modifiers are dropped when the carbonate content is > 60%. If the carbonate content is < 30%, the terrigenous, siliceous biogenic, or volcanogenic names apply, with the dominant carbonate type retained as a qualifier. Carbonate is not acknowledged in the name if it is present in amounts < 10%.

Terrigenous Sediments

The textural classification of terrigenous sediments (Fig. 20) follows that of Shepard (1954), with grain-size limits as defined by Wentworth (1922). Sediments and sedimentary rocks are assigned terrigenous names according to their textural classification when these components are > 30%. If the terrigenous component is between 30 and 60%, the biogenic or volcanogenic modifier is retained. For example, a nannofossil mud contains > 10% calcareous nannofossils and 30-60% silty clay, with sand-silt-clay proportions of 0-20:25-50: 50-75. The biogenic or volcanogenic modifier is dropped when that component is < 10%. For hard terrigenous sediments the suffix *stone* is added. Characteristic components are noted in smear slide or coarse-fraction descriptions.

Volcanogenic and Pyroclastic Sediments

We arbitrarily distinguish pyroclastic rocks from volcanogenic sediments, using 50% as the pivotal percentage, pyroclastic rocks having > 50%. Wentworth and Williams's (1932) textural and compositional classification applies for the pyroclastic rocks. Textural groups are as follows:

> 32 mm—volcanic breccia;

4-32 mm—volcanic lapilli (lapilli tuff when indurated);

< 4 mm—volcanic ash (tuff when indurated).

The compositional breakdown is *vitric* (glass), *crystalline*, or *lithic*, according to the most common con-

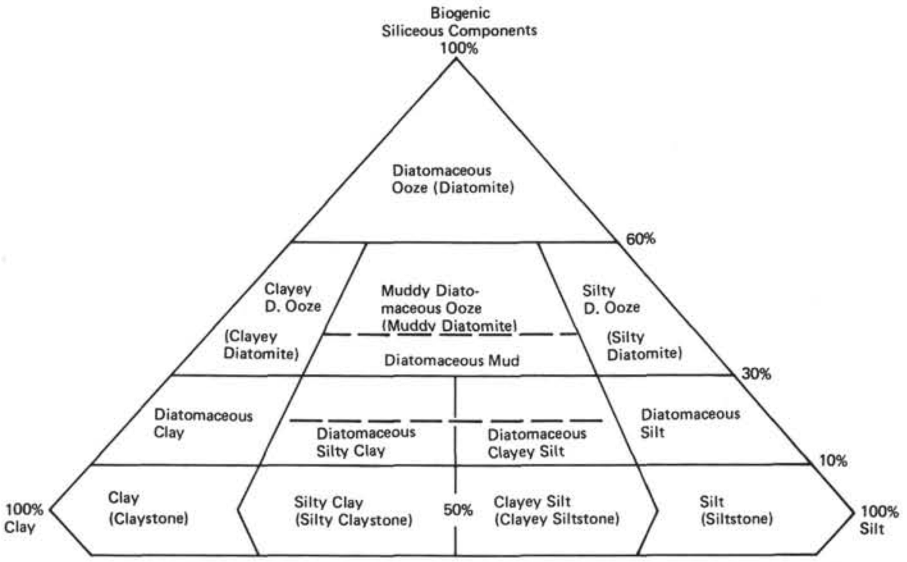

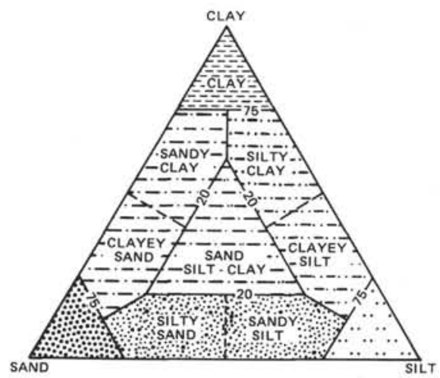

Figure 20. Hemipelagic and textural classification of clastic sediments (Shepard, 1954).

stituent. Qualifiers are used when volcanic components are between 50 and 90%. For example, "Clayey Vitric Ash" contains >10% clay and 50-90% ash composed mainly of glass shards. Terrigenous and biogenic modifiers are dropped if <10%.

When the volcanic component is <50%, the terminology and class boundaries for terrigenous (and, less often, biogenic) sediments apply. The modifier *tuffaceous* encompasses both ash and lapilli when either or both of these components occur in amounts between 10 and 50%. Thus "Tuffaceous Clayey Sand" (stone) contains 10-50% ash and/or lapilli and 50-90% clayey sand.

Hemipelagic Sediments

Figure 20 (top) shows the standard DSDP hemipelagic sediment classification.

Special Sediment and Sedimentary Rock Types

The special sediment types from Leg 74 are gravels, conglomerates, and breccias containing varying amounts of volcanogenic and biogenic sediments. Symbols are given in Figure 17.

BIOSTRATIGRAPHY

Nannofossil, planktonic, and benthic foraminifers were studied from all cores containing sediments. Biostratigraphic zonation of the Neogene (Fig. 21) is based on the time scales and zonations of Vincent (1977) and Martini (1971); of the Paleogene (Fig. 22) on the time scales and zonations of Hardenbol and Berggren (1978) and Martini (1971); and of the Cretaceous (Fig. 23) of the time scales and zonations of Thierstein (1976) and Sliter (unpublished).

Special Studies of Sediments

Organic Carbon and Carbonate Content

Measurements of organic carbon made on selected samples were done on board using the Hewlett-Packard CHN analyzer. In addition we selected samples to be analyzed at the DSDP sediment laboratory on a LECO WR-12 carbon analyzer. Some of the data were not available at the time of this compilation, but should be in the near future.

Carbonate content was determined on board using the "Carbonate Bomb" method already described. These data appear on the core description forms as "% $CaCO_3$."

Grain-Size Analysis

Sediment samples selected for grain-size analyses at the DSDP sedimentary laboratory, using standard sieve and pipette methods, were not available at the time of this compilation.

X-Ray Diffraction

An X-ray diffraction unit is now on board the *Glomar Challenger*. Preliminary XRD results are available upon request.

IGNEOUS ROCKS

Visual Core Description Forms

All igneous rocks were split by rock saw into working and archive halves described and sampled on board. Figure 24 shows a composite visual core description form used for the description of igneous rocks recovered on Leg 74. On this form, each section of a core is described under a set of five column headings: (1) Piece Number, (2) Graphic Representation, (3) Orientation, (4) Shipboard Studies, and (5) Alteration.

In the graphic representation column each piece is accurately drawn and different features, such as texture, glassy margins, or vesicles, coded according to the symbols given in Figure 25. Two closely spaced horizontal lines in this column indicate the location of styrofoam spacers taped between pieces inside the liner. Each piece is numbered sequentially, beginning with 1, from the top of each section. Pieces are labeled on the rounded, not the sawed, surface. Pieces which fit together before splitting are given the same number but are consecutively lettered (1A, 1B, 1C, etc.). Spacers were placed only between pieces which did not fit together; those pieces were given different numbers. In general, spacers may or may not indicate material missing (not recovered) between pieces. All cylindrical pieces longer than the diameter of the liner have arrows in the Orientation column, indicating that top and bottom have not been reversed as a result of drilling and recovery. Arrows also appear on their labels on both archive and working halves.

The Shipboard Studies column designates the location and the types of measurements made on a sample on board. The Alteration column gives the degree of alteration, using the code given in Figure 25. Below each set of five descriptive columns is the designation for core and section for which these data apply.

Figure 24 gives the outline for core descriptions of igneous rocks in the right-hand margin of the visual core description form. If more than one core appears on the form, these data are listed below the description of the first core, using the same format. As many cores as space allows are included on one visual core description form. Data that do not fit on this form appear on the verso or on a facing page. However, in no case does information from one core appear on successive core forms.

For each core, the core number, sections, and depth interval recovered are listed first, followed by the major and minor rock types and a short description, thin section data, and, finally, shipboard data.

Classification of Igneous Rocks

We informally classified igneous rocks recovered on Leg 74 according to mineralogy and texture determined from visual inspection of hand specimens and thin sections. The following conventions were agreed upon while at sea, and we realize they are generalized. It is possible that gradations exist within and among textural groups in a single sample.

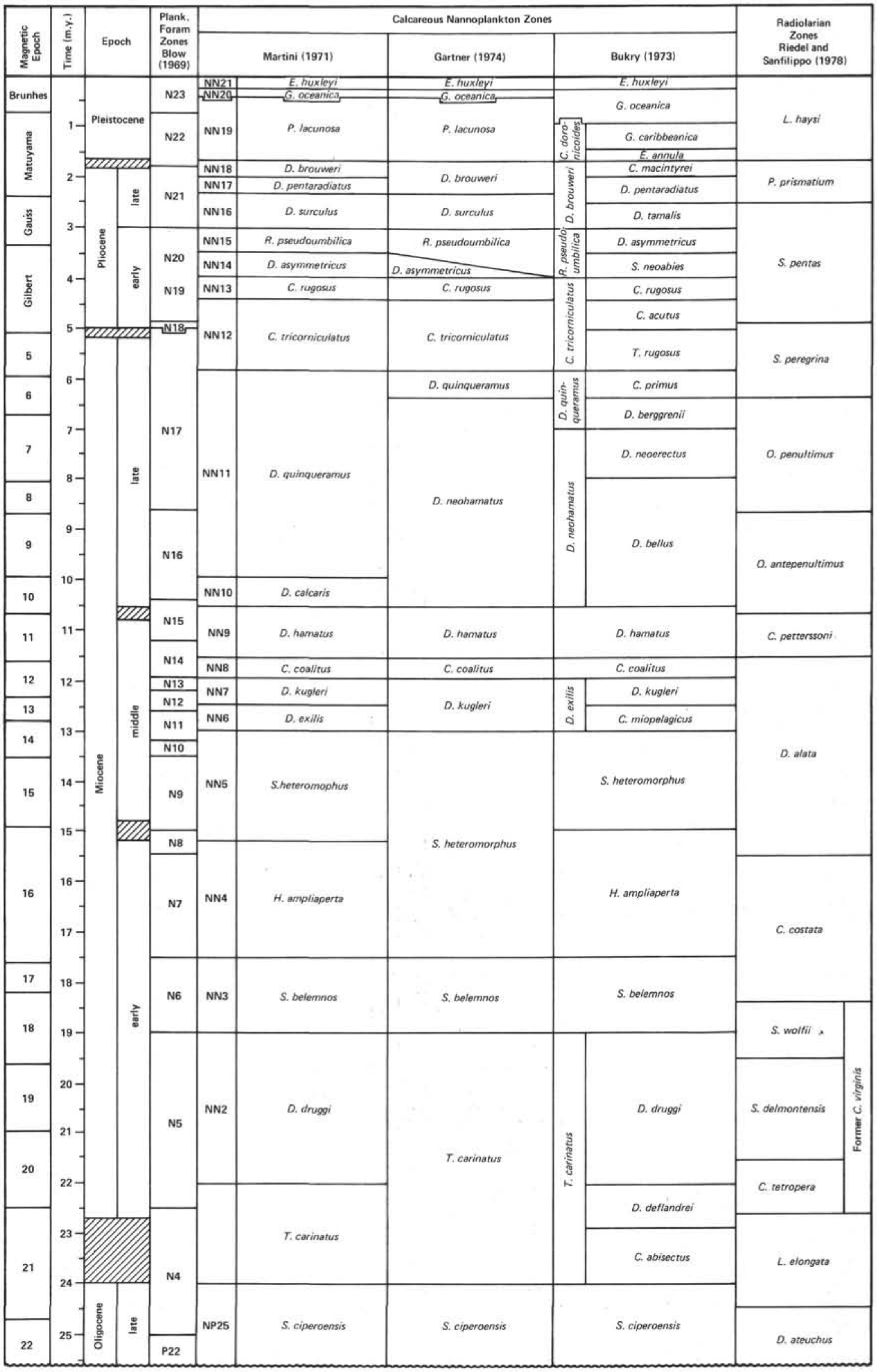

Figure 21. Biostratigraphic time scale and zonation of the Neogene, after Vincent (1977) and Martini (1971).

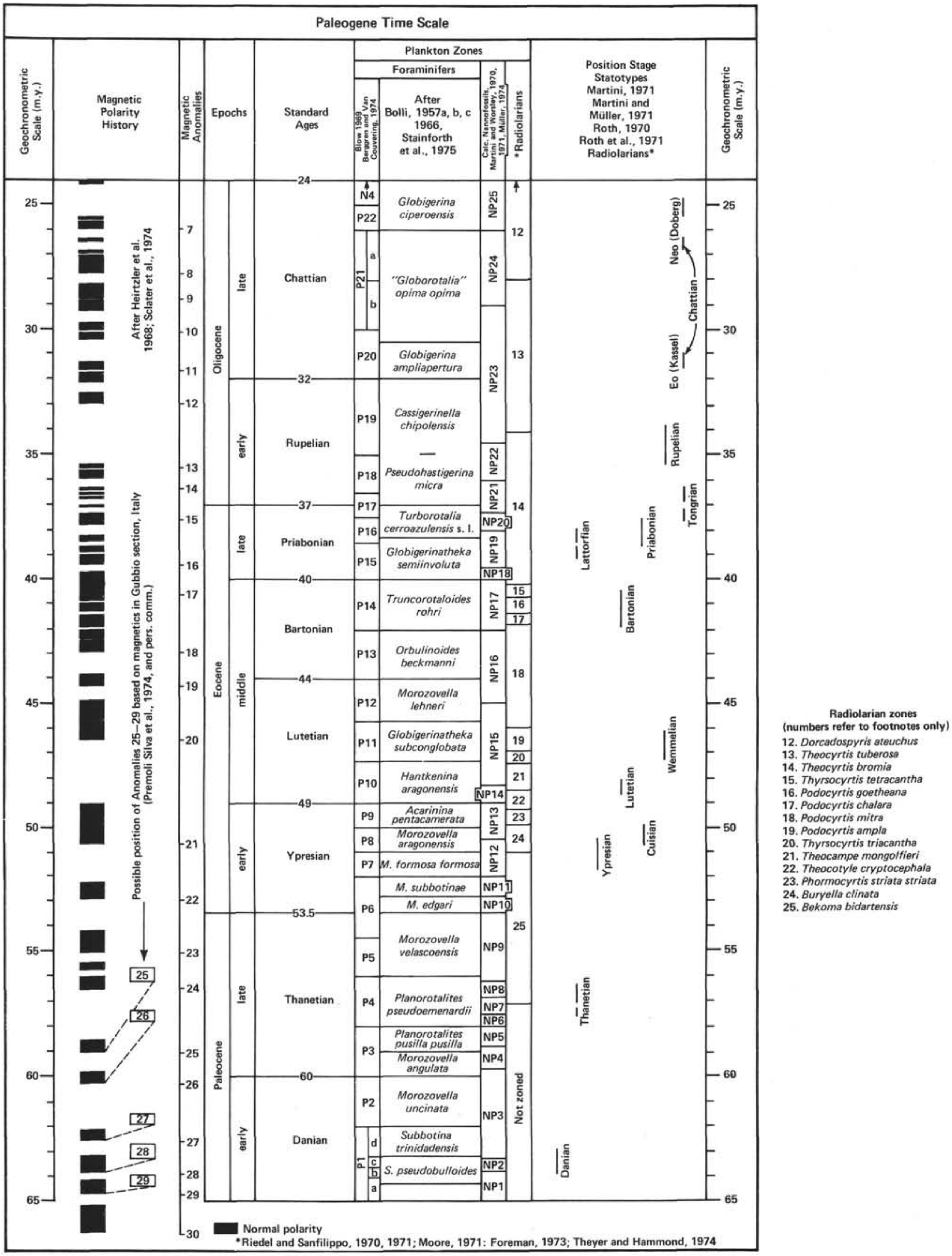

Figure 22. Biostratigraphic time scale and zonation of the Paleogene, after Hardenbol and Berggren (1978) and Martini (1971).

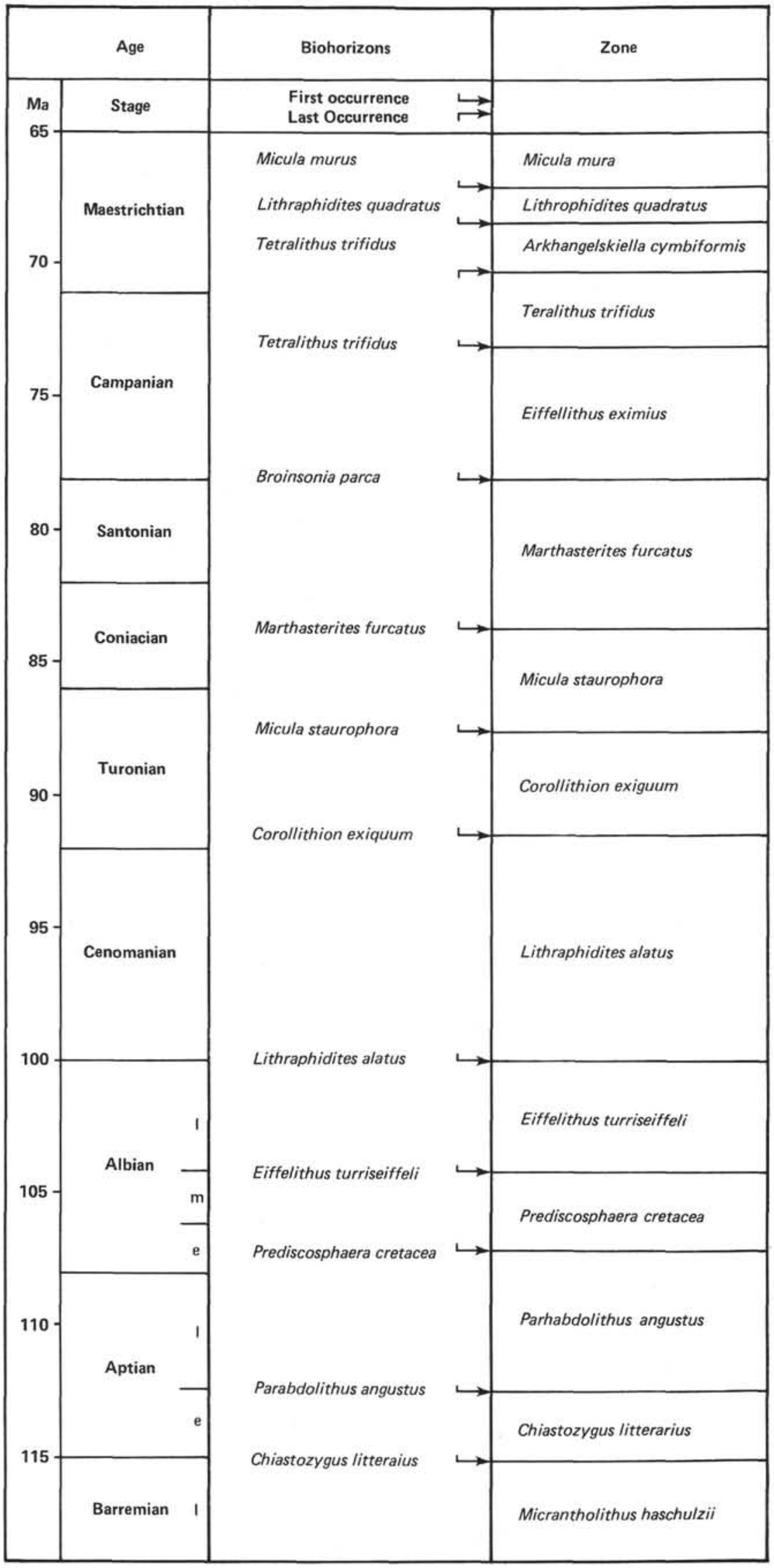

Figure 23. Biostratigraphic time scale and zonation of the Cretaceous, after Thierstein (1976) and Sliter (unpublished).

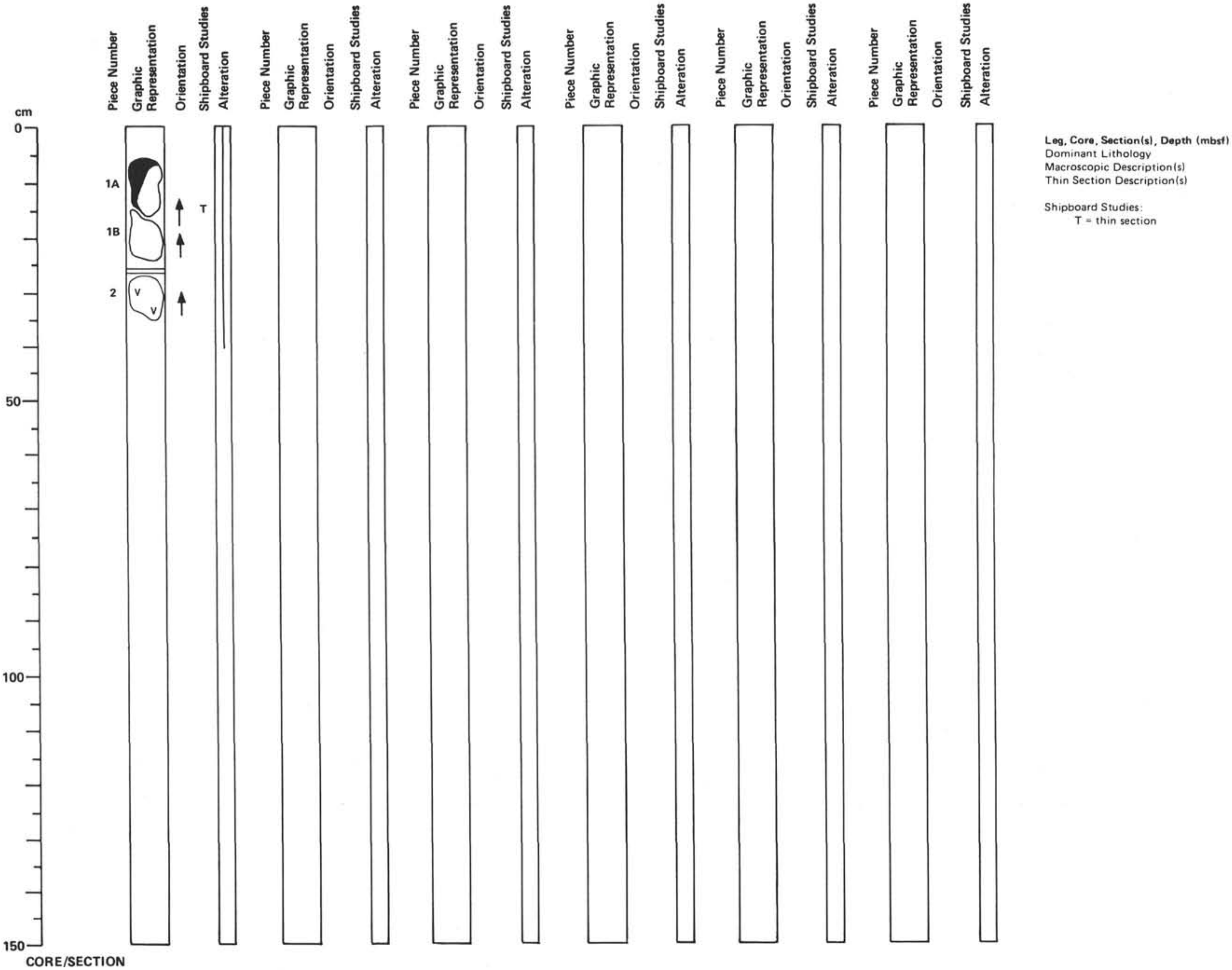

Figure 24. Visual core description form (igneous rock).

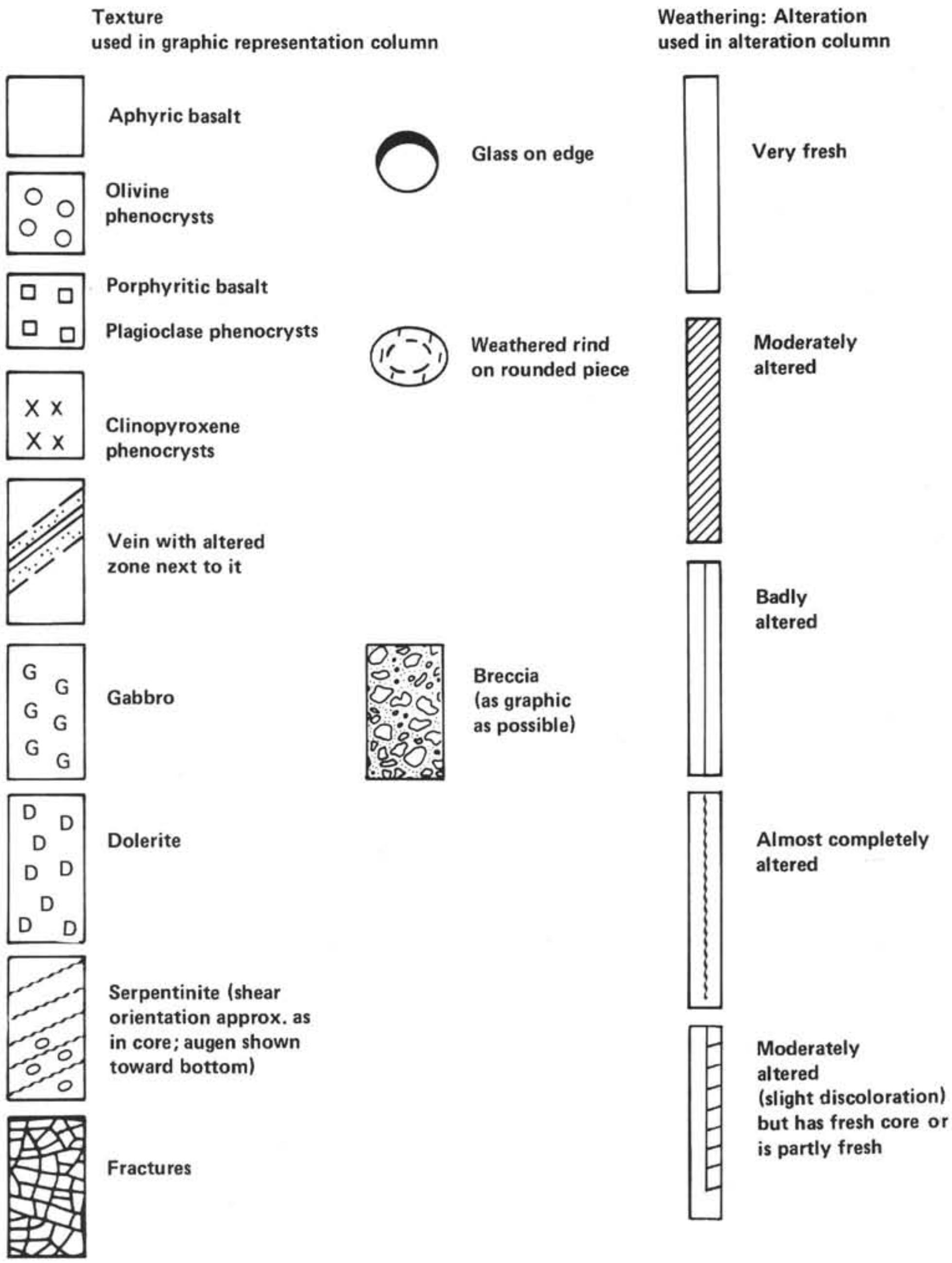

Figure 25. List of symbols for igneous rocks.

A. Quench textures recognized and described:
   1. Glassy—matrix is amorphous, basaltic glass with no visible, incipient crystallization.
   2. Variolitic—texture characterized by the presence of varioles, which are spherical bodies, usually consisting of radiating plagioclase and/or clinopyroxene microlites or crystals; individual crystals are indistinguishable with the microscope.
   3. Subvariolitic—texture in which varioles coalesce.
   4. Immature sheaf—a bundled arrangement of small crystals (which cannot be individually distinguished with the microscope) assuming a sheaflike appearance; a central axis of crystal growth often occurs.
   5. Mature sheaf—same as (4), but discrete skeletal crystals (usually >0.005 mm wide) can be distinguished with the microscope.
   6. Plumose—plume-or feather-like arrangement of microlites or crystals; may grade from immature to mature (as in sheaf texture) according to crystal size.

B. Major textural classification for basaltic samples used during Leg 74 includes the following terms:
   1. Phyric—describes igneous rocks in which larger crystals (phenocrysts) are set in a finer groundmass which may be crystalline or glassy, or both.
      Aphyric: no phenocrysts.
      Sparsely phyric: 1–2% phenocrysts.

Moderately phyric: 2–10% phenocrysts.
Highly phyric: >10% phenocrysts.

2. Glomerophyric—applied to phyric rocks containing clusters of equant crystals larger than the matrix crystals.
3. Ophitic—applied to a texture in which euhedral or subhedral crystals of plagioclase are embedded in a mesostasis of pyroxene crystals.
4. Subophitic—characterizing the ophitic texture of an igneous rock in which the feldspar crystals are approximately the same size as the pyroxene and only partially included by them.
5. Intergranular—applied to volcanic rocks in which there is an aggregation of clinopyroxene grains —not in parallel optical continuity (as in subophitic texture)—in a network of feldspar laths characterized by the absence of interstitial glass or other quenched places which may fill the interstices.
6. Intersertal—applied to volcanic rocks wherein a base of mesostasis or glass and small crystals fills the interstices between unoriented feldspar laths, the base forming a relatively small proportion of the rock. When the amount of the base increases and the feldspar laths decrease, the texture becomes hyalophitic; with still greater increase in the amount of the base, the texture becomes hyalopilitic.

Paleomagnetic data taken on board are not listed but will appear in a more comprehensive study by shipboard scientists.

PHYSICAL PROPERTIES

The following physical properties were determined routinely:

Measurement/Determination	Sediment	Basalt
Gravimetric procedure		
Bulk density	X	X
Water content	X	X
Porosity	X	X
Approximate grain density	X	X
Shrinkage	X	
Bulk density by 2-minute GRAPE	X	X
Vane shear strength	X	
Penetrometer strength	X	
Sonic velocity	X	X
Thermal conductivity	X	X

In general, we tried to perform these measurements at least once on every core. Water content samples were taken in every section unless the cores were highly disturbed. All samples were taken from, and measurements made on, the least disturbed section(s) of each core.

Gravimetric Procedure

The methods used here are described by Boyce (1976a). Bulk density and porosity were gravimetrically determined, either by the cylinder technique or by measuring chunks cut from the split core. The cylinder technique was used on soft or stiff sediments. Samples were taken with stainless steel or brass cylinders of known volume (about 5 cm^3 and 15 cm^3) and weight and were tightly enclosed until they could be weighed. On indurated sediment and hard rock, samples were cut in cube-shaped pieces from the split core halves and stored under seawater. Before the gravimetric measurements were made, sonic velocity and 2-minute GRAPE density were obtained on the samples (see GRAPE section). Their volume was determined by weighing both in air and suspended under water. A number of samples without defined volume were taken for determination of water content alone.

Sample volume and weight yield the wet-bulk density without a buoyancy correction. Wet water content and porosity were calculated from the water loss after drying at 110°C for 24 hr. Water content is related to the weight of the wet samples and therefore is defined here as wet-water content. All wet-water content and porosity data are corrected for salt content, using the correction factors for seawater (Boyce, 1976). The approximate grain density was calculated from the gravimetric data (as it is only an approximation, no correction for salt content was applied). The porosity is calculated assuming that the sediments are water-saturated. This may not be true of all samples, because some undergo adiabatic expansions if the *in situ* pressure is released when the cores are brought from the seafloor to the shipboard laboratory. The effect of the volume increase of the samples due to elastic rebound, caused by the removal of *in situ* overburden pressure (Hamilton, 1976), was not taken into account.

Shrinkage

Shrinkage is the loss of volume expressed as a percentage of the original volume ($vol._{wet}$) of the wet cylinder sample after drying at 110°C. The volume of the shrunken cylindrical sample ($vol._{shr.}$) was calculated from its mean height and diameter as determined by at least three caliper or dial micrometer measurements each of height and diameter. The shrinkage is defined as

$$S = \frac{vol._{wet} - vol._{shr.}}{vol._{wet}} \times 100\%.$$

The measurement is inaccurate, because after shrinkage most samples are not ideal cylinders. Nevertheless, the shrinkage data may provide valuable information with respect to composition and early diagenesis of the sediments.

GRAPE

Another method for determinating wet-bulk density is by the shipboard Gamma Ray Attenuation Porosity Evaluator (GRAPE). In addition to the continuous GRAPE density determinations on the unsplit core sections, special 2-minute counts were taken on either the cylinder samples (WCS samples for shorebased determination of gravimetric physical properties) or on the pieces of lithified material used for the shipboard gravimetric procedures (Boyce, 1976). On these pieces, GRAPE density could be measured in directions both parallel and perpendicular to the core axis. GRAPE porosity was not determined, because good porosity data could be obtained by gravimetric methods and because porosity determinations from GRAPE data may have a large error if grain density is not accurately known (Boyce, 1976).

Vane Shear and Penetrometer Strength

Shear strength was measured on the split core halves applying a torque to the sediment using the modified Wykeham Farrance Laboratory Vane Apparatus (Boyce, 1977). The vane used had an average height of 1.27 cm, a diameter of 1.28 cm, and a vane constant of 0.2273. The blades were buried about 0.5 cm below the sediment surface of the split core halves with the vane axis oriented parallel to the bedding plane of the sediment. A few determinations of remolded shear strength were performed.

Penetrometer measurements were made both by allowing the needle to drop from 1 cm directly above the sediment surface at 0 cm. The needle axis was oriented normal to the split half surface.

The determination both of vane shear strength and penetration was impossible when the sediments were indurated or lithified, as the sample cracked when the vane was inserted. At all sites only the upper two-thirds of the cored sediment sequence could be tested.

Sonic Velocity

Compressional sound velocity of both sediments and basaltic rocks was measured with the Hamilton Frame Velocimeter at 400 kHz (Boyce, 1976). By measuring aluminum, Lucite, and brass standards, the correction factors for the oscilloscope were determined at the beginning of Leg 74. They were $K = 0.99866$ for the 2-μs setting and $K = 1.00575$ for the 5-μs setting. These factors were applied on all sound velocity measurements. The sound velocity of weak sediments was determined parallel to bedding on split core halves, through the core liner, with corrections for liner thickness (2.56 mm) and travel time (1.18 μs) through it. On the indurated sediments and basalts, measurements of sonic velocity were made on the samples used for gravimetric procedure. The pieces were stored under seawater to prevent drying. Sonic velocity could be determined in horizontal (i.e., perpendicular to the core axis) and vertical (i.e., parallel to the core axis) directions. All samples were measured after they had reached room temperature.

Acoustic impedance was calculated as the product of sonic velocity and wet-bulk density, using both gravimetrically determined density data and GRAPE density values.

Thermal Conductivity

Thermal conductivity was determined using a needle thermistor probe (No. 28) on weak and stiff sediment and a flat needle block thermistor probe (No. 1) on indurated or lithified sediments and hard rock, following the shipboard laboratory manual. It was sometimes difficult to obtain a stable zero reading in air, and the instrument drift during measurement was often very large, which affected the quality of the data. Still, several control measurements performed on shipboard standards yielded reproducible data with an acceptable scatter (Table 4). Measurements were taken after the samples had come to equilibrium temperature.

Table 4. Thermal conductivity measurements of shipboard semistandards

	Blue Plastic Standard (used with needle probe No. 28)		Granite Standard (used with flat block probe No. 1)	Ceramic Standard No. 30146 (used with flat block probe No. 1)
	W/m°C	W/m°C	W/m°C	W/m°C
	2.50	1.48	3.03	3.36
	1.53	1.47	3.05	3.36
	1.50	1.48	3.02	3.33
	1.42	1.47	3.25	3.39
	1.70	1.39	3.09	3.35
	1.37	1.46	3.77	3.39
	2.24	1.46	3.68	3.37
	1.47	1.41	3.05	
	1.60	1.49		
	1.49			
Mean	$x = 1.58$		$x = 3.24$	$x = 3.36$
Standard deviation	$s = 0.29$		$s = 0.31$	$s = 0.01$

On unlithified sediments, thermal conductivity was measured on split core halves by inserting the needle probe obliquely into the sediment. This procedure is less time-consuming than inserting the probe through the unsplit liner, and it allows measurements at undisturbed sections of the core.

On indurated sediment and basalt, the flat block probe was used. Pieces of split core were stored in seawater while reaching room temperature. At times the section surface was ground to obtain a smooth interface. The measurement itself was performed with the probe and sample immersed in seawater.

PHOTOGRAPHY

As supplements to the core descriptions, sets of color and black and white slides and photographs of whole cores are available for consultation at both repositories. In addition, negatives in color and black and white for close-up documentation of special structures are archived at DSDP. Table 5 lists those from Leg 74. Photographs are available on a charge and time available basis.

DOWNHOLE LOGGING

Owing to bad weather and equipment failure the detailed logging program planned for Leg 74 was abbreviated. Nevertheless, we did successfully log holes at Sites 527 and 528. We obtained a density log at Site 527 and a sonic log with gamma ray traces at Site 528. A detailed analysis of the logging results is given in the respective site chapters and in Rabinowitz and Borella, this volume.

REFERENCES

Alvarez, W., Arthur, M. A., Fischer, A. G., Lowrie, W., Napoleone, G., Premoli-Silva, I., and Roggenthen, W. M., 1977. Upper Cretaceous–Paleocene magnetic stratigraphy at Gubbio, Italy v. type section from the late Cretaceous–Paleocene geomagnetic reversal time scale. *Geol. Soc. Am. Bull.*, 88:383–389.

Berger, W. H., 1977. Carbon dioxide excursions and the deep-sea record: aspects of the problem. *In* Anderson, R. N., and Malahoff, A. (Eds.), *The Fate of Fossil Fuel CO_2 in the Oceans:* New York (Plenum Press), pp. 505–542.

_______, 1978. Sedimentation of deep-sea carbonate: maps and models of variations and fluctuations. *J. Foram. Res.*, 8:286–302.

Berger, W. H., and Winterer, E. L., 1974. Plate stratigraphy and the flucuating carbonate line. *In* Hsü, K. J., and Jenkyns, H. S. (Eds.), *Pelagic Sediments on Land and under the Sea*. Spec. Publ. Int. Assoc. Sedimentol., 1:11–48.

Berggren, W. A., and Van Couvering, J. A., 1974. Biostratigraphy, geochronology, and paleoclimatology of the last 15 m.y. in marine and continental sequences. *Palaeogeogr. Palaeoclimatol., Palaeoecol.*, 16:1–216.

Bischoff, J. L., and Dickson, F. W., 1975. Sea water-basalts interaction at 200°C and 500 bars: Implications for origin of sea floor heavy metal deposits and regulation of sea water chemistry. *Earth Planet Sci. Lett.*, 25:385–397.

Blow, W. H., 1969. Late middle Eocene to Recent planktonic foraminiferal biostratigraphy. *In* Brönnimann, P., and Renz, H. H. (Eds.), *First Internat. Conf. Plankt. Microfossils*, 1:199–421.

Bolli, H. M., 1957a. The genera *Globigerina* and *Globorotalia* in the Paleocene-lower Eocene Lizard Springs Formation of Trinidad, B.W.I. *U.S. Natl. Mus. Bull.*, 215:61–81.

_______, 1957b. Planktonic Foraminifera from the Oligocene-Miocene Cipero and Lengua Formations of Trinidad, B.W.I. *U.S. Natl. Mus. Bull.*, 215:97–123.

_______, 1957c. Planktonic Foraminifera from the Eocene Navet and San Fernando Formations of Trinidad, B.W.I. *U.S. Natl. Mus. Bull.*, 215:155–172.

Boyce, R. E., 1976. Definitions and laboratory techniques of compressional sound velocity parameters and wet-water content, wet-bulk density, and porosity parameters by gravimetric and gamma ray attenuation techniques. *In* Schlanger, S. O., Jackson, E. D., et al., *Init. Repts. DSDP*, 33: Washington (U.S. Govt. Printing Office), 931–958.

_______, 1977. Deep Sea Drilling Project procedures for shear strength measurements of clayey sediment using modified Wykeham Farrance laboratory vane apparatus. *In* Barker, P. F., Dalziel, I. W. D., et al., *Init. Repts. DSDP*, 36: Washington (U.S. Govt. Printing Office), 1059–1068.

Bukry, D., 1973. Coccolith stratigraphy, Leg 13, Deep Sea Drilling Project. *In* Ryan W. B. F., Hsü, K. J., et al., *Init. Repts. DSDP.*, 13, Pt. 2: Washington (U.S. Govt. Printing Office), 817–822.

Chave, R. D., 1979. Lithospheric structure of the Walvis Ridge from Rayleigh wave dispersion. *J. Geol. Res.*, 84:6840–6848.

Connary, S. D., and Ewing, M., 1974. Penetration of Antarctic Bottom Water from the Cape Basin into the Angola Basin. *J. Geophys. Res.*, 79:463–469.

Detrick, R. S., and Watts, A. B., 1979. An analysis of isostasy in the world's oceans. 3. Aseismic ridges. *J. Geophys. Res.*, 84 (No. B7): 3637–3655.

Foreman, H. P., 1973. Radiolaria of Leg 10 with systematics and ranges for the families Amphipyndacidae, Artostrobiidae, and Theoperidae. *In* Worzel, J. L., Bryant, W., et al., *Init. Repts. DSDP*, 10: Washington (U.S. Govt. Printing Office), 407–474.

Gealy, E. L., Winterer, E. L., and Moberly, R., 1971. Methods, conventions, and general observations. *In* Winterer, E. L., Riedel W. R., et al., *Init. Repts. DSDP*, 7, Pt. 1: Washington (U.S. Govt. Printing Office), 9–26.

Goslin, J., and Sibuet, J.-C., 1975. Geophysical study of the easternmost W. R., South Atlantic: deep structure. *Geol. Soc. Am. Bull.*, 86:1713–1724.

Hamilton, E. L., 1976. Variations of density and porosity with depth in deep-sea sediments. *J. Sediment. Petrol.*, 46:280–300.

Hardenbol, J., and Berggren, W. A., 1978. A new Paleogene numerical time scale. *Am. Assoc. Petrol. Stud. Geol.*, 6:213–234.

Heirtzler, J. R., Dickson, G. O., Herron, E. M., Pitman, W. C., and LePichon, X., 1968. Marine magnetic anomalies, geomagnetic field reversals, and motions of the ocean floor and continents. *J. Geophys. Res.*, 73(6):2119–2136.

Martini, E., 1970. Standard Paleogene calcareous nannoplankton zonation. *Nature*, 266(5245):560–561.

_______, 1971. Standard Tertiary and Quaternary calcareous nannoplankton zonation. *In* Farinacci, A. (Ed.), *Proc. II Plankt. Conf. Roma:* Rome (Edizione Tecnoscienzia), pp. 739–785.

Martini, E., and Worsley, T., 1970. Standard Neogene calcareous nannoplankton zonation. *Nature*, 225(5229):289–290.

Moore T., 1971. Radiolaria. *In* Tracy J. I., Jr., Sutton G. H., et al., *Init. Repts. DSDP*, 8: Washington (U.S. Govt. Printing Office), 727–775.

Müller, C., 1974. Calcareous nannoplankton, Leg 25 (Western Indian Ocean). *In* Simpson, E. S. W., Schlich, R., et al., *Init. Repts, DSDP*, 25: Washington (U.S. Govt. Printing Office), 579–633.

Müller, G., and Gastner, M., 1971. The "Karbonate Bomb," a simple device for determination of the carbonate content in sediments, soils, and other materials. *Neues Johrb. Miner. Monatsh.*, 10: 466–469.

Ness, G., Levi, S., and Crouch, R., 1980. Marine magnetic anomaly time scales for the Cenozoic and Late Cretaceous: a precis, critique, and synthesis. *Rev. Geophys.*, 18:753–770.

Premoli-Silva, I., Napoleone, G., and Fisscher, A. G., 1974. Risultati preliminari sulla stratigrafia paleomagnetica della scaglia Cretaceo-Paleocenia della sezione di Gubbio (Appennino centrale). *Soc. Geol. Italiana Boll.*, 93:64–659.

Rabinowitz, P. D., and LaBrecque, J., 1979. The Mesozoic South Atlantic Ocean and evolution of its continental margins. *J. Geophys. Res.*, 84(No. B11):5973–6002.

Rabinowitz, P. D., and Simpson, E. S. W., 1979. Results of IPOD site surveys aboard R/V *Thomas B. Davie:* Walvis Ridge survey. *L-DGO Tech. Rept.*, JOI, Inc.

Riedel, W. R., and Sanfilippo, A., 1970. Radiolaria, Leg 4, DSDP. *In* Bader, R. G., Gerard, R. D., et al., *Init. Repts. DSDP*, 4: Washington (U.S. Govt. Printing Office), 503–575.

_______, 1971. Cenozoic Radiolaria from the western tropical Pacific, Deep Sea Drilling Project, Leg VII. *In* Winterer, E. L., Riedel, W. R., et al., *Init. Repts. DSDP*, 7, Pt. 2: Washington, (U.S. Govt. Printing Office), 1529–1672.

_______, 1978. Stratigraphy and evolution of tropical Cenozoic radiolarians. *Micropaleontology*, 24(1):61–96.

Sclater, J. G., Jarrard, R. D., McGowran, B., and Gartner, S. 1974. Comparison of the magnetic and biostratigraphic time scales since the Late Cretaceous. *In* von der Borch, C. C., Sclater, J. G., et al., *Init. Repts. DSDP*, 22: Washington (U.S. Govt. Printing Office), 381–386.

Shephard, F. P., 1954. A scale of grade and class terms of clastic sediments. *J. Geol.*, 30:337.

Stainforth, R. M., 1975. Cenozoic planktonic foraminiferal zonation and characteristics of index forms. *Univ. Kansas Paleont. Contr.* 62:1–45.

Takahashi, T., 1975. Carbonate chemistry of sea water and the calcite compensation depth in the oceans. *In* Sliter, W. V., Bé, A. W. H., and Berger, W. H. (Eds), *Cushman Found. Foram. Res.*, 13: 11–26.

Theyer, F., and Hammond, S. R., 1974. Paleomagnetic polarity sequence and radiolarian zones, Brunhes to polarity Epoch 20. *Earth Planet. Sci. Lett.*, 22:307–319.

Thierstein, H. R., 1976. Mesozoic calcareous nannoplankton biostratigraphy of marine sediments. *Mar. Micropaleont.*, 1:325–362.

Vincent, E., 1977. Indian Ocean Neogene planktonic foraminiferal biostratigraphy and its paleoceanographic implications. *In* Heirtzler, J. R., Bolli, H. M., Davies, T. A., et al. (Eds.), *Indian Ocean Geology and Biostratigraphy:* Washington (Am. Geophys. Union), pp. 469–548.

Wentworth, C. K., 1922. A scale of grade and class terms of clastic sediments. *J. Geol.*, 30:337.

Wentworth, C. K., and Williams, H., 1932. The classification and terminology of the pyroclastic rocks. *Rept. Comm. Sedimentation, Bull. Nat. Res. Covnc.*, 80:10–53.

Wüst, G., 1936. Das Bodenwasser und die Gliedering der Atlantischen Tiefsee. *Wiss. Ergeb. Dtsch. Atl. Exped. Meteor.*, 1925–1927, 6(1):3–107.

Table 5. Leg 74 detail core photographs (black and white).

Negative No.	Sample (interval in cm)	Negative No.	Sample (interval in cm)
1	525-22-6, 100–115	32	528-29-2, 55–60
2	525A-42-2, 5–20	33	528-29-2, 65–75
3	525A-40-2, 0–25	34	528-29-4, 42–52
4	525A-41-4, 72–83	35	528-29-4, 60–80
5	525A-51-2, 35–50	36	528-29-4, 79–90
6	526A-2-3, 50–65	37	528-30-2, 43–63
7	526A-2-3, 85–100	38	528-30-2, 60–80
8	527-13-2, 70–80	39	528-30-4, 52–62
9	527-13-3, 75–95	40	528-31-2, 19–29
10	527-13-3, 115–130	41	528-31-5, 69–76
11	527-14-4, 70–95	42	528-33-1, 22–41
12	527-14-4, 95–120	43	528-33-1, 126–129
13	527-14-4, 120–145	44	528-33-1, 135–139
14	527-24-2, 15–40	45	528-43-1, 64–74
15	527-24-2, 40–65	46	528A-2-2, 71–91
16	527-30-1, 132–145	47	529-8-5, 130–135
17	527-30-2, 35–50	48	529-33-3, 19–40
18	527-31-1, 145–150	49	529-33-3, 90–107
19	527-32-4, 40–60	50	529-33-3, 135–150
20	527-36-4, 110–125	51	529-34-3, 115–135
21	527-37-5, 60–75	52	529-35-1, 20–30
22	527-41-5, 40–68	53	529-36-3, 140–150 (A)
23	528-4-4, 55–70	54	529-36-3, 140–150 (top)
24	528-4-4, 95–115	55	529-36-3, 140–150 (mid)
25	528-4-4, 115–135	56	529-36-3, 140–150 (btm)
26	528-16-3, 32–38	57	529-36-4, 65–75
27	528-17-3, 70–80	58	529-40-2, 90–100
28	528-28-1, 10–20	59	529-41-1, 5–15
29	528-28-1, 20–26	60	529-42-1, 10–35
30	528-28-2, 35–48	61	529-42-2, 70–85
31	528-29-2, 20–25		